Molecular Neurobiology (2019) 56:3835–3853
https://doi.org/10.1007/s12035-018-1118-5

PARK14 (D331Y) PLA2G6 Causes Early-Onset Degeneration of Substantia Nigra Dopaminergic Neurons by Inducing Mitochondrial Dysfunction, ER Stress, Mitophagy Impairment and Transcriptional Dysregulation in a Knockin Mouse Model

Ching-Chi Chiu[1,2,3] · Chin-Song Lu[1,3,4,5] · Yi-Hsin Weng[1,3,4,5] · Ying-Ling Chen[2] · Ying-Zu Huang[1,3,4,5,6] · Rou-Shayn Chen[1,3,4,5] · Yi-Chuan Cheng[7] · Yin-Cheng Huang[5,8] · Yu-Chuan Liu[9] · Szu-Chia Lai[1,3,4,5] · Kun-Jun Lin[1,10] · Yan-Wei Lin[1,4] · Yu-Jie Chen[1] · Chao-Lang Chen[1] · Tu-Hsueh Yeh[11,12] · Hung-Li Wang[1,3,4,13]

Received: 4 January 2018 / Accepted: 11 May 2018 / Published online: 8 August 2018

Abstract

PARK14 patients with homozygous (D331Y) PLA2G6 mutation display motor deficits of pure early-onset Parkinson's disease (PD). The aim of this study is to investigate the pathogenic mechanism of mutant (D331Y) PLA2G6-induced PD. We generated knockin (KI) mouse model of PARK14 harboring homozygous (D331Y) PLA2G6 mutation. Then, we investigated neuropathological and neurological phenotypes of PLA2G6$^{D331Y/D331Y}$ KI mice and molecular pathogenic mechanisms of (D331Y) PLA2G6-induced degeneration of substantia nigra (SN) dopaminergic neurons. Six-or nine-month-old PLA2G6$^{D331Y/D331Y}$ KI mice displayed early-onset cell death of SNpc dopaminergic neurons. Lewy body pathology was found in the SN of PLA2G6$^{D331Y/D331Y}$ mice. Six-or nine-month-old PLA2G6$^{D331Y/D331Y}$ KI mice exhibited early-onset parkinsonism phenotypes. Disrupted cristae of mitochondria were found in SNpc dopaminergic neurons of PLA2G6$^{D331Y/D331Y}$ mice. PLA2G6$^{D331Y/D331Y}$ mice displayed mitochondrial dysfunction and upregulated ROS production, which may lead to activation of apoptotic cascade. Upregulated protein levels of Grp78, IRE1, PERK, and CHOP, which are involved in activation of ER stress, were found in the SN of PLA2G6$^{D331Y/D331Y}$ mice. Protein expression of mitophagic proteins, including parkin and BNIP3, was downregulated in the SN of PLA2G6$^{D331Y/D331Y}$ mice, suggesting that (D331Y) PLA2G6 mutation causes mitophagy dysfunction. In the SN of PLA2G6$^{D331Y/D331Y}$ mice, mRNA levels of eight genes that are involved in neuroprotection/neurogenesis were decreased, while

Electronic supplementary material The online version of this article (https://doi.org/10.1007/s12035-018-1118-5) contains supplementary material, which is available to authorized users.

✉ Tu-Hsueh Yeh
do2739@gmail.com

✉ Hung-Li Wang
hlwns@mail.cgu.edu.tw

1 Neuroscience Research Center, Chang Gung Memorial Hospital at Linkou, Linkou, Taoyuan, Taiwan

2 Department of Nursing, Chang Gung University of Science and Technology, Taoyuan, Taiwan

3 Healthy Aging Research Center, Chang Gung University College of Medicine, Taoyuan, Taiwan

4 Division of Movement Disorders, Department of Neurology, Chang Gung Memorial Hospital at Linkou, Taoyuan, Taiwan

5 College of Medicine, Chang Gung University, Taoyuan, Taiwan

6 Institute of Cognitive Neuroscience, National Central University, Taoyuan, Taiwan

7 Graduate Institute of Biomedical Sciences, Chang Gung University College of Medicine, Taoyuan, Taiwan

8 Department of Neurosurgery, Chang Gung Memorial Hospital at Linkou, Taoyuan, Taiwan

9 Division of Sports Medicine, Taiwan Landseed Hospital, Taoyuan, Taiwan

10 Molecular Imaging Center, Chang Gung Memorial Hospital at Linkou, Taoyuan, Taiwan

11 Department of Neurology, Taipei Medical University Hospital, No. 252, Wuxing St, Xinyi District, Taipei City 110, Taiwan

12 School of Medicine, Taipei Medical University, Taipei, Taiwan

13 Department of Physiology and Pharmacology, Chang Gung University College of Medicine, No. 259, Wen-Hwa 1st Road, Kweishan, Taoyuan 333, Taiwan

mRNA levels of two genes that promote apoptotic death were increased. Our results suggest that PARK14 (D331Y) PLA2G6 mutation causes degeneration of SNpc dopaminergic neurons by causing mitochondrial dysfunction, elevated ER stress, mitophagy impairment, and transcriptional abnormality.

Keywords Parkinson's disease · PARK14 · (D331Y) PLA2G6 · Knockin mice

Introduction

Parkinson's disease (PD) is a common neurodegenerative disorder caused by progressive degeneration of dopaminergic neurons in substantia nigra pars compacta (SNpc) [1]. The pathological hallmark of PD is Lewy bodies in surviving SNpc dopaminergic cells [2]. Although the exact etiology of PD remains unveiled, mitochondrial dysfunction, endoplasmic reticulum (ER) stress, inflammation, oxidative stress, and impaired autophagy are believed to be implicated in the pathogenesis of PD [3, 4].

Patients affected with autosomal recessive PARK14 display early-onset parkinsonism [5]. Mutations of PLA2G6 (Ca^{2+}-independent phospholipase A_2 group 6) gene cause PLA2G6-associated neurodegeneration (PLAN), including infantile neuroaxonal dystrophy, atypical neuroaxonal dystrophy, neurodegeneration with brain iron accumulation, and young-onset PARK14 [6]. Previous studies by us and other research groups reported that a homozygous c.991G>T (p.Asp331Tyr, D331Y) mutation in PLA2G6 is the genetic cause of PARK14 patients [7–9]. Patients with homozygous (D331Y) PLA2G6 mutation display motor dysfunctions of pure early-onset autosomal recessive PD [7–9]. Knockin mouse model is the useful tool to investigate the pathogenesis of Parkinson's disease caused by mutant PLA2G6. Up to now, knockin mouse expressing PARK14 (D331Y) PLA2G6 has not been used to investigate the pathogenic mechanism of (D331Y) PLA2G6-induced PD.

PLA2G6 hydrolyzes the sn-2 acyl group of phospholipid to produce lysophospholipids and free fatty acids. Released fatty acid, including arachidonic acid, causes the formation of leukotrienes, lipoxins, or prostaglandins, which activate signal transduction pathways [10]. PLA2G6 participates in several cellular functions such as mitochondrial function, fatty acid oxidation, calcium signaling, cell growth, apoptosis, and gene regulation [11, 12]. Deficiency of PLA2G6 in Drosophila results in mitochondrial membrane defects, mitochondrial dysfunction, and peroxidation of mitochondrial lipid [13]. PLA2G6 knockout mice exhibit the degeneration of mitochondrial inner membrane [14]. PLA2G6 deficiency in mice also causes autophagy impairment [15].

In this study, we prepared knockin (KI) mouse harboring homozygous (D331Y) PLA2G6 mutation and studied the molecular mechanism of (D331Y) PLA2G6-induced Parkinson's disease. The results of our investigation provide the evidence that PARK14 mutant (D331Y) PLA2G6 induces early-onset degeneration of SNpc dopaminergic neurons by causing mitochondrial dysfunction, ER stress, mitophagy impairment, and transcriptional dysregulation.

Materials and Methods

Generation of PLA2G6$^{D331Y/\ D331Y}$ Knockin Mice

PCR-based site-directed mutagenesis was conducted to alter the codon GAC for Asp-331 located in the exon 7 of mouse PLA2G6 gene into TAC encoding Tyr. Then, exon 7 fragment with (D331Y) mutation was subcloned into pBluescript SK vector. For the knockin target vector of PLA2G6^{D331Y}, a neomycin selection cassette flanked by LoxP sites was inserted at site of 401 nucleotides downstream the start of exon 7. To target the exon 7, 4.9-kb fragment upstream of exon 7 and 2.2-kb fragment downstream of neomycin selection cassette were obtained and functioned as 5′ and 3′ homologous arms, respectively. Subsequently, knockin targeting fragments of PLA2G6^{D331Y} were subcloned into pBluescript vector containing mutated exon 7 fragment and LoxP-flanked neomycin selection cassette.

The 129/Sv embryonic stem (ES) cells were transfected with XhoI-linearized knockin target vector of PLA2G6^{D331Y}. PCR assays were performed to screen neomycin-resistant colonies with correct homologous recombination. Chimeric mice were obtained by microinjecting correctly targeted ES clone into C57BL/6J blastocysts. F1 heterozygous mutant mice were bred from wild-type C57BL/6J mice and chimeric mice. To remove Neo cassette, F1 mice with germline transmission of (D331Y) PLA2G6 knockin allele were bred with Cre deleter transgenic mice, which express Cre recombinase in the whole body. Then, stable lines of mutant (D331Y) PLA2G6 knockin mice were established by mating F2 PLA2G6$^{WT/D331Y}$ mice with wild-type C57BL/6J mice. The resultant heterozygous knockin mice were bred and maintained on C57BL/6J genetic background and intercrossed to generate homozygous PLA2G6$^{D331Y/D331Y}$ knockin mice. Animal experiments were performed in accordance with protocols approved by Institutional Animal Care and Use Committee (IACUC) of Chang Gung University.

Subcellular Fractionation

Cytosolic and mitochondrial fractions of SN dissected from WT or KI mice were prepared. Briefly, SN tissues were

homogenized in ice-cold buffer comprising 10 mM HEPES (pH 7.3), 1 mM DTT, 1 mM EGTA, 70 mM sucrose, 210 mM mannitol, and commercial protease inhibitor cocktail (Sigma). Cell lysate was centrifuged at 500×*g* for 10 min at 4 °C. Then, the supernatant was collected and centrifuged at 9500×*g* for 10 min at 4 °C to obtain the pellet, which was mitochondrial fraction. The supernatant was further centrifuged at 16,000×*g* for 20 min at 4 °C to obtain cytosolic fraction.

Western Blot

Mitochondrial or cytosolic proteins (30 μg) were separated on a 12 or 15% SDS-polyacrylamide gel and then transferred onto nitrocellulose membranes. Subsequently, membranes were incubated overnight at 4 °C with following primary antibodies: (1) monoclonal anti-PLA2G6 antibody (Santa Cruz Biotechnology, sc-376563); (2) polyclonal anti-phospho-alpha synuclein^{Ser129} antiserum (Abcam, ab51253); (3) polyclonal anti-alpha synuclein antibody (Proteintech, # 10842-1-AP); (4) monoclonal anti-Tau antiserum (Santa Cruz Biotechnology, sc-32274); (5) monoclonal anti-phospho-Tau (Ser202, Thr205) antibody (Thermo Scientific, AT8); (6) polyclonal anti-BiP/Grp78 antiserum (Cell Signaling Technology, #3177); (7) polyclonal anti-CHOP antibody (Cell Signaling Technology, #2895); (8) polyclonal anti-IRE1α antiserum (Cell Signaling Technology, #3294); (9) polyclonal anti-PERK antibody (Cell Signaling Technology, #5683); (10) polyclonal anti-cleaved caspase-9 antiserum (Cell Signaling Technology, #20750); (11) polyclonal anti-cytochrome c antibody (Abcam, ab133504); (12) polyclonal anti-cleaved caspase-3 antibody (Cell Signaling Technology, #9662); (13) monoclonal anti-BMP6 monoclonal antiserum (Santa Cruz Biotechnology, sc-57042); (14) monoclonal anti-CCND2 antibody (Thermo Fisher Scientific, clone DCS3.1); (15) monoclonal anti-CTNNB1 antiserum (Millipore, clone 8E7); (16) polyclonal anti-GDNF antibody (Abcam, ab18956); (17) polyclonal anti-HSPA1B antiserum (Sigma, SAB1403949); (18) polyclonal anti-KIDINS220 antibody (Abcam, ab34790); (19) polyclonal anti-MAPK1 antiserum (Santa Cruz Biotechnology, sc-292838); (20) polyclonal anti-MARK4 antibody (Cell Signaling Technology, #4834); (21) polyclonal anti-PSAP antiserum (GeneTex, GTX101064); (22) monoclonal anti-SDC2 antibody (Santa Cruz Biotechnology, sc-376160); (23) polyclonal anti-XAF1 antiserum (GeneTex, GTX51339); (24) monoclonal anti-parkin antibody (Cell Signaling Technology, #4211); (25) monoclonal anti-BNIP3 antiserum (Cell Signaling Technology, #44060). Membranes were incubated with appropriate horseradish peroxidase-conjugated secondary antibodies. Then, chemiluminescence kit (Millipore) was used to visualize immunoreactive proteins. The density of gel bands was determined with a densitometer and normalized by actin signals.

Measurement of PLA2G6 Enzyme Activity

The modified cPLA$_2$ assay kit (Cayman Chemicals, Cat.765021) was used to analyze the phospholipase A$_2$ activity of PLA2G6 in the SN tissues. According to the stereotaxic atlas of mouse brain [16], SN was dissected out from coronal midbrain brain slices (500 μm) under a microscope. Then, SN tissues were lysed in a modified Ca^{2+}-depleted lysis buffer containing 50 mM HEPES (pH 7.4), 0.1% CHAPS, 4 mM EDTA, and commercial protease inhibitor cocktail (Sigma). The substrate arachidonoyl thio-phosphatidylcholine was incubated with protein sample in a modified Ca^{2+}-depleted lysis buffer (2 mg/mL bovine serum albumin, 8 mM Triton X-100, 160 mM HEPES (pH 7.4), 300 mM NaCl, 4 mM EGTA, 60% glycerol, and 8 mM Triton X-100) for 60 min at room temperature. Arachidonoyl thio-phosphatidylcholine was hydrolyzed by iPLA$_2$ and produced free thiols, which were detected by 5,5 o-dithiobis, 2-nitrobenzoic acid. The absorbance at 414 nm was measured and used to calculate the activity of iPLA$_2$.

Immunohistochemical Staining

Animals were anesthetized and intracardially perfused with 4% paraformaldehyde in 0.01 M PBS. Then, cryostat sectioned brain slices were incubated with anti-phospho-α-synuclein^{Ser129} polyclonal antibody, monoclonal anti-α-synuclein antibody, anti-NeuN monoclonal antibody, or monoclonal anti-tyrosine hydroxylase antibody. After the washes, brain slices were incubated with biotinylated secondary antibody (Vector Laboratories) and then incubated with streptavidin peroxidase conjugates. Subsequently, brain sections were visualized by incubating with diaminobenzidine (Vector Laboratories). The Stereo Investigator software (MBF Biosciences) was used to calculate the number of NeuN$^+$-neurons or TH$^+$-dopaminergic neurons. ImageJ software (National Institutes of Health) was used to quantify the striatal density of TH$^+$ staining.

Animal Image Study with ^{18}F-FP-DTBZ microPET

Animal imaging study utilizing a positron emission tomography (PET) imaging was acquired by an Inveon preclinical small animal PET scanner (Siemens Medical Solutions) at Molecular Imaging Center of Chang Gung Memorial Hospital. After receiving a single bolus injection of ^{18}F-FP-DTBZ (12.9 ± 1.47 MBq in 0.1 mL saline), mice were anesthetized with isoflurane, and images were acquired in 3D mode for 90 min. PET images were reconstructed using two-dimensional ordered-subset expectation maximum method without corrections for attenuation, randomness,

and scatter. Imaging data were processed and analyzed with PMOD software (PMOD Technologies, version 3.2). PET images were coregistered to the corresponding MRI imaging. Regions of interest were drawn within the striatum and cerebellum. Cerebellum was used for the reference region. The striatal specific uptake ratio (SUVR) was calculated as (the uptake of right of left striatum)/the uptake of cerebellum uptake.

Behavioral Assessments

The locomotor activity of WT or (D331Y) PLA2G6 KI mice was evaluated in open field boxes for 60 min. Movements of animal were recorded and assessed with the TopScan video tracking system (Clever Sys., Inc.). The locomotor activity of mouse was examined by measuring the velocity and distance. To evaluate the therapeutic benefit of L-DOPA in PLA2G6$^{D331Y/D331Y}$ mice, benserazide (0.5 mg/kg) and L-DOPA (1.5 mg/kg) were intraperitoneally administered into animal. The locomotor activity was recorded 40 min after the injection.

The motor performance of animal was assessed by the pole test. Mouse was placed on top of the pole, and the base of pole was positioned in the home cage. Animals oriented themselves downward and descended along the pole back into home cage. Animals received two consecutive days of training consisting of five trials for each session. On the day of pole test, animals carried out five trials. Motor performance of animal was determined by measuring the time needed for orienting downward and descending.

Rotarod test using an accelerating rotarod apparatus (Ugo Basile Biological Research Apparatus) was conducted to assess motor coordination and balance of animal. Briefly, mouse was placed on the accelerated rotarod, and the latency to fall off the rod was recorded.

Spontaneous movements of animals were analyzed by performing cylinder test. Animals were placed into an acrylic cylinder (12.7 cm diameter; 15.5 cm height), and the number of spontaneous rearing movements was recorded for 3 min.

Transmission Electron Microscopy Study

Mouse was intracardially perfused with 4% paraformaldehyde/2.5% glutaraldehyde fixative. The SN region of brain tissue was cut into 1-mm^3 slices by using a vibratome and post-fixed in 1% osmium tetroxide for 2 h. After 0.1 M phosphate buffer washing, SN slices were dehydrated through an ascending series of ethanol solutions and embedded in Epon resin (Electron Microscopy Sciences). Following sectioning, ultrathin (80 nm) sections were visualized using transmission electron microscope (JEM-1230, JEOL). The diameters of mitochondria were measured by using ImageJ software.

Determination of Intracellular ATP Content

Luminescent ATP determination kit (Thermo Fisher Scientific, Cat.A22066) was used to measure cellular level of ATP. Cell lysates (20 μL) were loaded in microplate and incubated with reaction buffer. Luminescence was determined by measuring the absorbance at 560 nm using TECAN luminescence reader (TECAN Infinite M200 Pro).

Measurement of Mitochondrial Complex I, Complex II, Complex III, or Complex IV Activity

The complex I enzyme activity assay kit (Abcam) was used to analyze the complex I activity of mitochondria. Mitochondrial extracts (50 μg) were added and incubated in microplate containing monoclonal anti-complex I antibody. The complex I activity was determined by measuring the oxidation of reduced NADH to NAD^+, which results in an increased absorbance at 450 nm.

The activity of mitochondrial complex II was determined by using complex II enzyme activity microplate assay kit (Abcam) following the manufacturer's instructions. Briefly, complex II of mitochondrial sample was immunocaptured within the microplate well, which was coated with an anti-complex II monoclonal antibody. Succinate was used as a substrate during performing this assay. The formation of ubiquinol by complex II caused the reduction of the dye DCPIP (2,6-diclorophenolindophenol), and a decrease in the absorbance of DCPIP at 600 nm was detected spectrophotometrically.

Mitochondrial complex III activity was determined by using mitochondrial complex III activity assay kit (BioVision) according to the manufacturer's instructions. Briefly, standard curve for various amounts of reduced cytochrome c was constructed by measuring the absorbance at 550 nm. Mitochondrial samples were added to reaction mixture with or without antimycin A. Following the addition of substrate cytochrome c, the absorbance at 550 nm was measured. The activity of complex III was determined by comparing OD values of samples with the standard curve of reduced cytochrome c.

The enzyme activity of mitochondrial complex IV was measured by using complex IV rodent enzyme activity microplate assay kit (Abcam) following the manufacturer's instructions. Briefly, complex IV of mitochondrial extract was immunocaptured within the sample well of microplate. Following the oxidation of reduced cytochrome c, the activity of complex IV was measured colorimetrically by the change of absorbance at 550 nm.

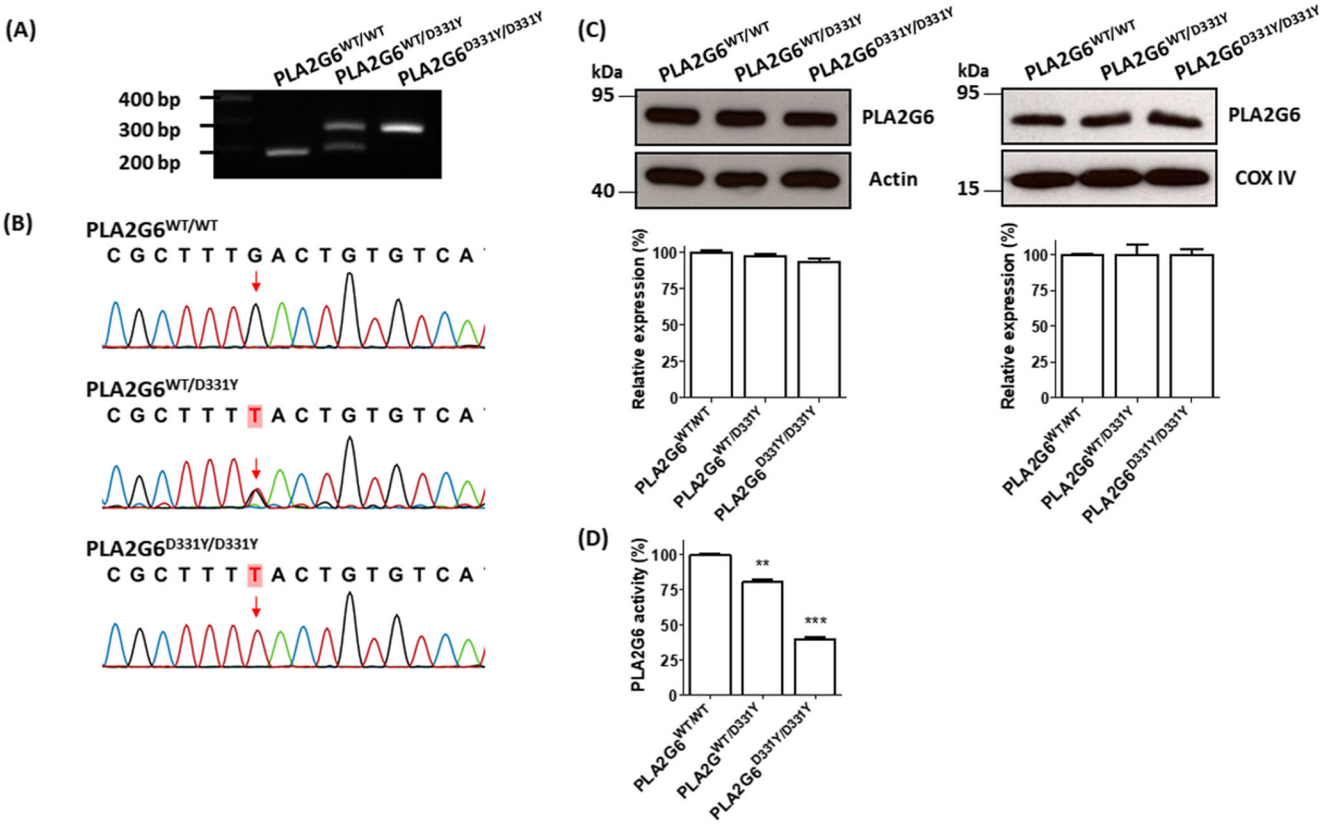

Fig. 1 The enzyme activity of PLA2G6 is significantly reduced in the SN of PLA2G6$^{D331Y/D331Y}$ knockin mice. **a** PCR assays were performed to genotype wild-type mice, PLA2G6$^{WT/D331Y}$ mice, and PLA2G6$^{D331Y/D331Y}$ mice. **b** Sanger sequencing of cDNA synthesized from the SN of PLA2G6$^{WT/D331Y}$ or PLA2G6$^{D331Y/D331Y}$ mice verified the (G991 → T991) nucleotide mutation at the residue D331 of PLA2G6. As a result, D331 (GAC) was converted to Y331 (TAC). **c** Western blot analysis using anti-PLA2G6 antibody showed that cytosolic or mitochondrial protein level of PLA2G6 in the SN of heterozygous (D331Y) PLA2G6 mice or homozygous (D331Y) PLA2G6 mice was similar to that of PLA2G6 in the SN of wild-type mice. **d** The enzyme activity of PLA2G6 was reduced in the SN of PLA2G6$^{WT/D331Y}$ mice or PLA2G6$^{D331Y/D331Y}$ mice compared to that of wild-type mice. Data are presented as mean ± SEM of 20 mice. $^{**}P < 0.01$, $^{***}P < 0.001$ compared with wild-type mice

Determination of Reactive Oxygen Species

OxiSelect In Vitro ROS/RNS assay kit (Cell Biolabs) was used to determine the level of reactive oxygen species (ROS). Mitochondrial extracts (50 μL) were loaded into microplate and incubated with 50 μL of the catalyst reagent, which accelerates the oxidative reaction. Following the incubation for 5 min, specific ROS probe DCFH-DiOxyQ was added into the mixture. DCFH-DiOxyQ oxidized by ROS generated fluorescent product dichlorofluorescein (DCF). Fluorescence intensity of DCF was measured with TECAN Infinite M200 Pro microplate reader.

Analysis of Mitochondrial Lipid Peroxidation

Thiobarbituric acid reactive substances (TBARS) assay kit (Cayman Chemicals, Cat.10009055) was used to examine the level of mitochondrial lipid peroxidation by quantifying the amount of malondialdehyde (MDA)-thiobarbituric acid (TBA) adduct. The formation of MDA-TBA adduct occurred under acidic conditions and high temperature. MDA standards or mitochondrial samples interacted with TBA at 100 °C for 60 min. The amounts of MDA-TBA adducts were then quantified by measuring optical density at 540 nm.

Measurement of Cytochrome c Release

Cytochrome c ELISA Assay Kit (Thermo Fisher Scientific, Cat.KHO1051) was used to evaluate the release of cytochrome c. Mitochondrial or cytosolic lysates were added into microplate containing monoclonal anti-cytochrome c antibody, followed by adding biotin conjugates. After incubation with streptavidin-HRP working solution, the substrate tetramethylbenzidine was loaded into microplate. Then, the optical density at 450 nm was measured.

Microarray Study

Total RNA was purified from substantia nigra of wild-type or PLA2G6$^{D331Y/D331Y}$ KI mice using RNeasy Mini Kit (Qiagen). Affymetrix Mouse Genome arrays were used to analyze gene expression profile. Eight samples (wild-type

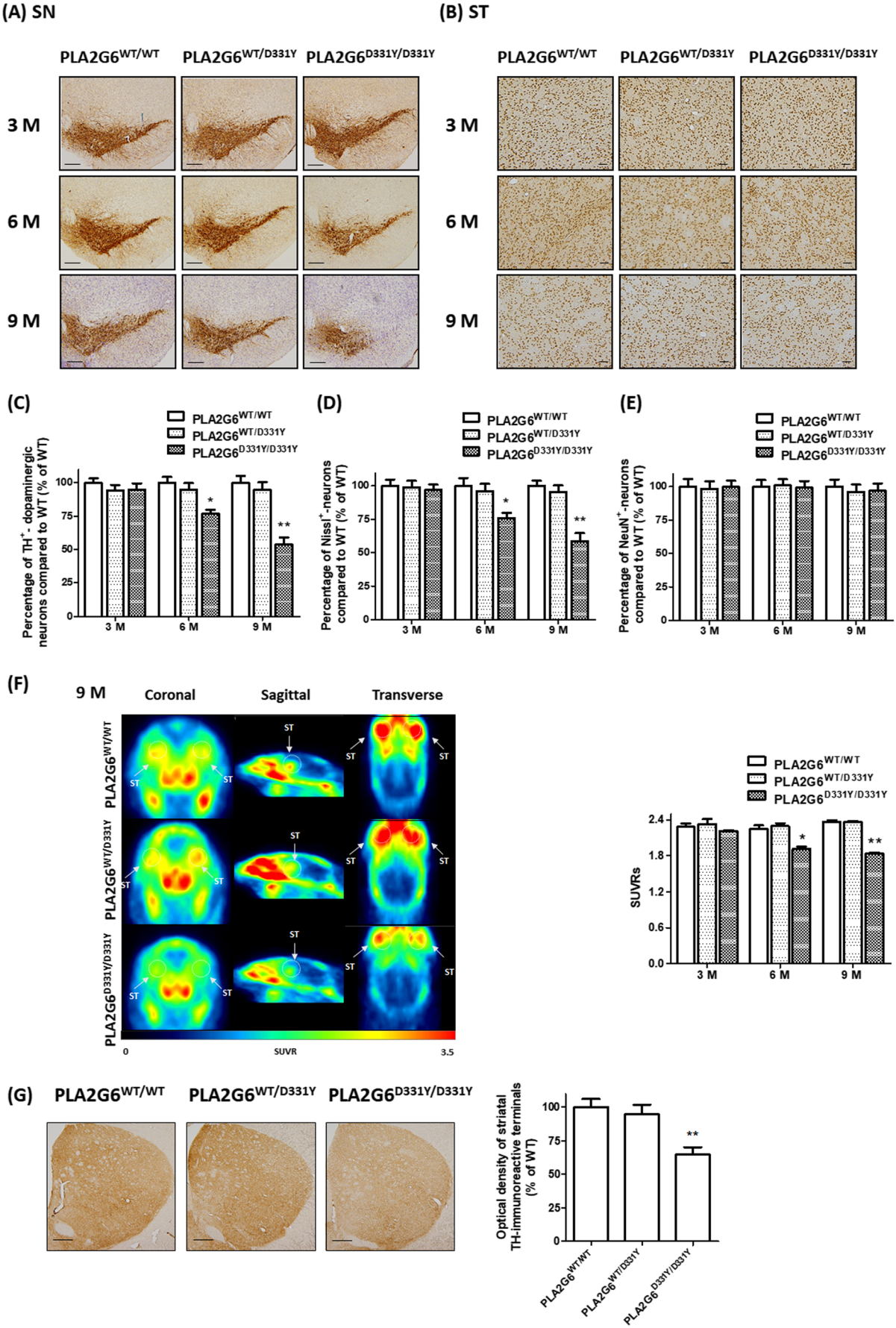
(A) SN
(B) ST
PLA2G6WT/WT
PLA2G6WT/D331Y
PLA2G6D331Y/D331Y
3 M
6 M
9 M
(C)
Percentage of TH+- dopaminergic neurons compared to WT (% of WT)
(D)
Percentage of Nissl+-neurons compared to WT (% of WT)
(E)
Percentage of NeuN+-neurons compared to WT (% of WT)
(F)
9 M
Coronal
Sagittal
Transverse
ST
SUVR
0
3.5
SUVRs
(G)
Optical density of striatal TH-immunoreactive terminals (% of WT)

◀ **Fig. 2** PLA2G6$^{D331Y/D331Y}$ KI mice display neuronal death of SNpc dopaminergic cells and the loss of nigrostriatal dopaminergic terminals. **a**, **c** TH immunostaining demonstrated that compared to age-matched WT mice or heterozygous PLA2G6$^{WT/D331Y}$ mice, the number of TH$^+$-dopaminergic neurons was significantly reduced in the SNpc of PLA2G6$^{D331Y/D331Y}$ KI mice at the age of 6 or 9 months. Scale bar is 200 μm. Each bar shows the mean ± SEM of 20 mice. **d** Six- or 9-month-old PLA2G6$^{D331Y/D331Y}$ knockin mice displayed a significantly decrease in the number of SNpc Nissl$^+$ cells. Each bar represents the mean ± SEM of 20 mice. **b**, **e** Immunohistochemical staining of NeuN demonstrated the absence of a significant neurodegeneration in the striatum of PLA2G6$^{D331Y/D331Y}$ KI mice. Scale bar is 200 μm. Each bar shows the mean ± SEM of 20 mice. **f** The VMAT2 density of striatal dopaminergic nerve terminals was visualized by performing in vivo ^{18}F-FP-DTBZ microPET imaging. Compared to WT or PLA2G6$^{WT/D331Y}$ mice, striatal ^{18}F-FP-DTBZ uptake of PLA2G6$^{D331Y/D331Y}$ knockin mice at the age of 6 or 9 months was significantly decreased. Ear bar represents the mean ± SEM of six mice. **g** Compared with age-matched WT mice or heterozygous PLA2G6$^{WT/D331Y}$ mice, 9-month-old PLA2G6$^{D331Y/D331Y}$ KI mice displayed a significant decrease in striatal density of TH-immunoreactive staining. Scale bar is 200 μm. Each bar represents as the mean ± SEM of 20 mice. *$P < 0.05$, **$P < 0.01$ compared with wild-type mice

mice, $n = 4$; PLA2G6$^{D331Y/D331Y}$ KI mice, $n = 4$) were prepared and analyzed. Differentially expressed genes were analyzed using the dCHIP software. Differential gene expression was estimated by the mean (PLA2G6$^{D331Y/D331Y}$/WT) expression ratio. The selection criteria for significantly altered gene expressions were $p < 0.05$ and fold change ≥ 1.9.

Real-Time Quantitative RT-PCR Assay

Quantitative real-time RT-PCR was performed on StepOne Real-Time PCR system (Applied Biosystems). The mRNA level of genes was normalized to reference gene GAPDH. The $2^{-(\Delta\Delta Ct)}$ equation was used to calculate the relative change of mRNA expression.

Statistics

Data were expressed as the mean ± SEM. One-way ANOVA followed by post-hoc Tukey's multiple comparison test was used to analyze statistical significance among multiple groups. Significant difference between two groups was determined by unpaired Student's *t* test (two-tailed). A *P* value of less than 0.05 was considered significant.

Results

PLA2G6$^{D331Y/D331Y}$ Homozygous Knockin Mice Exhibit a Decreased PLA2G6 Activity in the Substantia Nigra

To generate knockin mice expressing PARK14 mutant (D331Y) PLA2G6, we introduced human (D331Y; GAC→TAC) mutation in the exon 7 of mouse PLA2G6 gene by knockin target vector-mediated homologous recombination. The resultant heterozygous PLA2G6$^{WT/D331Y}$ knockin mice were bred and intercrossed to generate wild-type mice, heterozygous PLA2G6$^{WT/D331Y}$ mice, and homozygous PLA2G6$^{D331Y/D331Y}$ knockin mice (Fig. 1a). RT-PCR assay using total RNA purified from substantia nigra (SN) and Sanger sequencing was performed to confirm (D331Y) PLA2G6 mutation (Fig. 1b).

PLA2G6 is localized in the cytosol and mitochondria. Cytosolic protein expression of PLA2G6 in the SN of PLA2G6$^{WT/D331Y}$ or PLA2G6$^{D331Y/D331Y}$ mice was similar to that of PLA2G6 in the SN of WT mice (Fig. 1c). Mitochondrial protein expression of PLA2G6 in the SN of PLA2G6$^{WT/D331Y}$ or PLA2G6$^{D331Y/D331Y}$ mice was also not significantly altered (Fig. 1c). Compared to the enzyme activity of PLA2G6 in the SN of wild-type mice, heterozygous or homozygous (D331Y) PLA2G6 mutation led to a significant decrease in PLA2G6 enzyme activity (Fig. 1d). These results indicated that (D331Y) PLA2G6 mutation causes the loss of function.

PLA2G6$^{D331Y/D331Y}$ KI Mice Display Early-Onset Degeneration of SNpc Dopaminergic Neurons

Homozygous (D331Y) PLA2G6 mutation causes early-onset autosomal recessive PD [7–9]. We performed immunohistochemical tyrosine hydroxylase (TH) staining using 3- to 9-month-old heterozygous or homozygous (D331Y) PLA2G6 mice. The number of TH$^+$-SNpc dopaminergic cells of PLA2G6$^{D331Y/D331Y}$ knockin mice at the age of 3 months was not significantly different from that of age-matched PLA2G6$^{WT/D331Y}$ or WT mice (Fig. 2a, c). Compared with WT mice, 6- or 9-month-old homozygous PLA2G6$^{D331Y/D331Y}$ mice exhibited a significant reduction in the number of TH$^+$-SNpc dopaminergic cells (Fig. 2a, c). PLA2G6$^{WT/D331Y}$ mice did not display cell death of TH$^+$-SNpc dopaminergic neurons (Fig. 2a, c). Six- or nine-month-old PLA2G6$^{D331Y/D331Y}$ mice exhibited a significant reduction in the number of Nissl$^+$-cells of SNpc (Fig. 2d and Fig. S1). Immunocytochemical staining of NeuN, a neuronal marker, demonstrated that neuronal loss was not found in the striatum (Fig. 2b, e), hippocampus, and cerebral cortex (Fig. S2A and S2B) of PLA2G6$^{D331Y/D331Y}$ mice.

PLA2G6$^{D331Y/D331Y}$ Knockin Mice Display the Loss of Nigrostriatal Dopaminergic Terminals

The radiotracer ^{18}F-FP-DTBZ binds to vesicular monoamine transporter type 2. PET imaging with ^{18}F-FP-DTBZ was conducted to monitor the integrity of nigrostriatal dopaminergic terminals in animal model of PD and PD patients. The microPET imaging analysis demonstrated that 3-month-old

PLA2G6$^{D331Y/D331Y}$ KI mice did not display a significant decrease in the striatal uptake of ^{18}F-FP-DTBZ (Fig. 2f). Compared to 6- or 9-month-old WT mice, the striatal uptake of ^{18}F-FP-DTBZ was significantly reduced in age-matched PLA2G6$^{D331Y/D331Y}$ KI mice (Fig. 2f). Compared to 9-month-old WT mice, the density of striatal TH staining in age-matched PLA2G6$^{D331Y/D331Y}$ mice was significantly decreased (Fig. 2g).

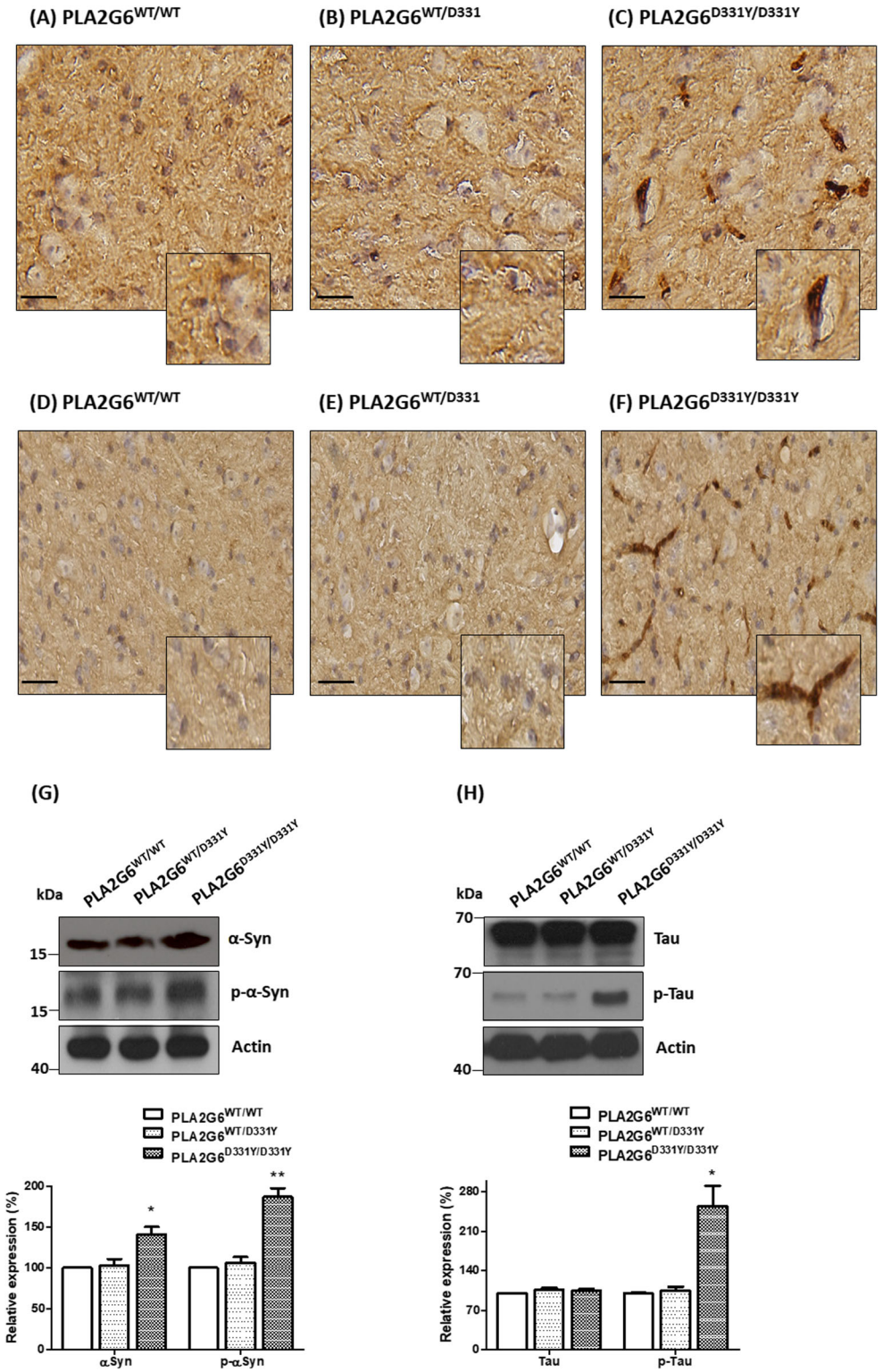

◀ **Fig. 3** Lewy body pathology is found in the SN o PLA2G6$^{D331Y/D331Y}$ KI mice at the age of 9 months. **a**–**f** Lewy body in the SN of PLA2G6$^{D331Y/D331Y}$ KI mice at the age of 9 months was detected by performing immunocytochemical staining of anti-p-αSyn (**a**–**c**) and anti-αSyn (**d**–**f**). Scale bar is 50 μm. **g** Immunoblotting analysis showed an upregulated protein expression of αSyn or p-αSyn in the SN of homozygous PLA2G6$^{D331Y/D331Y}$ KI mice at the age of 9 months. The same observation was found in other four experiments. **h** The expression of tau protein (Tau) in SN of PLA2G6$^{D331Y/D331Y}$ mice was similar to PLA2G6$^{WT/WT}$ mice. Immunoblotting assay demonstrated that an increased protein level of phospho-tau$^{Ser202/Thr205}$ (p-Tau) was found in the SN of homozygous PLA2G6$^{D331Y/D331Y}$ mice at the age of 9 months. The expression level of proteins was quantified by the densitometer. The same observation was found in other four experiments. Each bar shows the mean ± SEM value of five independent experiments. $^{*}P < 0.05$, $^{**}P < 0.01$ compared with wild-type mice

PLA2G6$^{D331Y/D331Y}$ KI Mice Exhibit Lewy Body-like Pathology

Lewy body, which is mainly composed of α-synuclein (αSyn), phosphorylated α-synuclein, and other components, is the neuropathological hallmark of Parkinson's disease [1]. Immunohistochemical staining using anti-phospho-α-synuclein^{Ser129} (p-αSyn) (Fig. 3a–c) antiserum and anti-αSyn antibody (Fig. 3e, f) demonstrated that Lewy bodies were found in the SN of PLA2G6$^{D331Y/D331Y}$ mice at the age of 9 months. Immunoblotting analysis demonstrated that PLA2G6$^{D331Y/D331Y}$ KI mice at the age of 9 months displayed an upregulated protein expression of αSyn and p-αSyn (Fig. 3g). Immunofluorescence staining showed that the formation of αSyn aggregates was observed in the TH^{+}-SN dopaminergic neuron of PLA2G6$^{D331Y/D331Y}$ mice (Fig. S3 of Supplementary material). Lewy body-like inclusions can be biochemically analyzed in sarkosyl-insoluble fraction [17, 18]. To confirm α-synuclein pathology, the accumulation of αSyn and p-αSyn was examined in the sarkosyl-insoluble fraction obtained from the SN of (D331Y) PLA2G6 KI mice. Biochemical analysis showed that accumulation of αSyn and p-αSyn was observed in the sarkosyl-insoluble fractions of homozygous (D331Y) PLA2G6 KI mice (Fig. S4 of Supplementary material). PD patients with PLA2G6 mutations exhibit an increased protein level of hyperphosphorylated tau, which is the tau pathology [19]. Western blot analysis indicated that protein expression of phospho-tau$^{Ser202/Thr205}$ was upregulated in the substantia nigra of PLA2G6$^{D331Y/D331Y}$ mice (Fig. 3h).

PLA2G6$^{D331Y/D331Y}$ Knockin Mice Exhibit Early-Onset and Progressive Parkinsonism Phenotypes

Six- to 12-month-old PLA2G6$^{D331Y/D331Y}$ mice exhibited an early-onset and progressive decrease in the locomotion activity, including the velocity (Fig. 4a) and distance (Fig. 4b). The cylinder test was conducted to analyze spontaneous movements of mice. Six- to 12-month-old PLA2G6$^{D331Y/D331Y}$ mice displayed a significant decrease in the number of rears (Fig. 4c). Motor coordination of animal was evaluated by performing the rotarod test. Six- to 12-month-old PLA2G6$^{D331Y/D331Y}$ knockin mice displayed an impaired motor coordination, which was indicated by a marked reduction in retention time on the rotarod apparatus (Fig. 4d). The pole test was conducted to examine the motor performance of animal. Six- to 12-month-old PLA2G6$^{D331Y/D331Y}$ KI mice displayed an increase in time required to perform the pole test, which indicated impaired motor performance and bradykinesia phenotype (Fig. 4e).

L-DOPA was effective in treating PD patients carrying PLA2G6 mutations [20]. Similar to PARK14 patients, treatment of methyl L-DOPA rescued hypoactivity displayed by 9-month-old PLA2G6$^{D331Y/D331Y}$ knockin mice (Fig. 4f, g).

Homozygous (D331Y) PLA2G6 KI Mice Exhibit Mitochondrial Degeneration and Mitochondrial Dysfunction

The ultrastructure of mitochondria in the neuromelanin organelle-containing SNpc dopaminergic neuron was examined by performing transmission electron microscopy. Intact morphology and well-defined cristae of mitochondria were observed in the neuromelanin-positive putative SNpc dopaminergic cells of WT mice or heterozygous PLA2G6$^{WT/D331Y}$ mice ($n = 20$ neurons). In contrast, disrupted cristae of mitochondria were found in the neuromelanin organelle-containing putative SN dopaminergic neurons of PLA2G6$^{D331Y/D331Y}$ knockin mice ($n = 20$ neurons) (Fig. 5a–c). Moreover, the mitochondrial size was decreased in the SN of homozygous (D331Y) PLA2G6 mice compared to WT or heterozygous (D331Y) PLA2G6 mice (Fig. 5d).

Abnormal ultrastructure of mitochondria could lead to mitochondrial dysfunction. An impaired activity of mitochondrial complex I activity is found in PD patients [21]. The activities of mitochondrial complex I-IV were analyzed in the SN of homozygous (D331Y) PLA2G6 KI mice. Compared with WT mice, the activity of mitochondrial complex I or III was reduced in the SN of PLA2G6$^{D331Y/D331Y}$ mice (Fig. 5e, g). The activity of mitochondrial complex II or IV was not significantly altered in the SN of PLA2G6$^{D331Y/D331Y}$ mice (Fig. 5f, h). A reduced level of intracellular ATP production was also found in the SN of PLA2G6$^{D331Y/D331Y}$ mice (Fig. 5i).

Mitochondrial dysfunction causes the overproduction of ROS and lipid peroxidation. Cardiolipin, a unique mitochondrial phospholipid, participates in maintaining mitochondrial function and cytochrome c release [22]. ROS generated from mitochondria results in the oxidation of cardiolipin and subsequent activation of apoptosis through the release of cytochrome c [22]. The status of cardiolipin oxidation can be

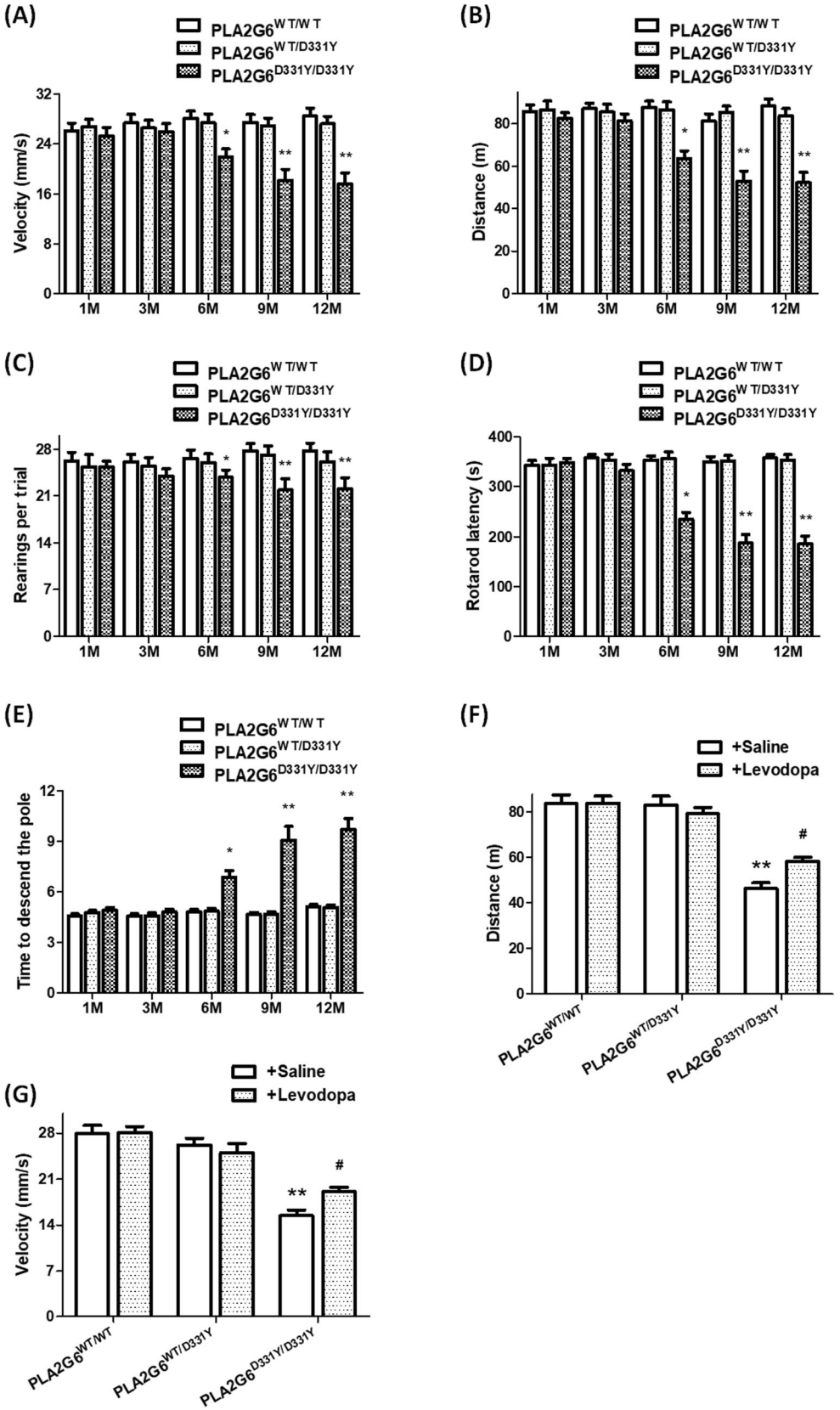
(A)
PLA2G6W T/W T
PLA2G6W T/D331Y
PLA2G6D331Y/D331Y
Velocity (mm/s)
32
24
16
8
0
1M
3M
6M
9M
12M
*
**
**
(B)
PLA2G6W T/W T
PLA2G6W T/D331Y
PLA2G6D331Y/D331Y
Distance (m)
80
60
40
20
0
1M
3M
6M
9M
12M
*
**
**
(C)
PLA2G6W T/W T
PLA2G6W T/D331Y
PLA2G6D331Y/D331Y
Rearings per trial
28
21
14
7
0
1M
3M
6M
9M
12M
*
**
**
(D)
PLA2G6W T/W T
PLA2G6W T/D331Y
PLA2G6D331Y/D331Y
Rotarod latency (s)
400
300
200
100
0
1M
3M
6M
9M
12M
*
**
**
(E)
PLA2G6W T/W T
PLA2G6W T/D331Y
PLA2G6D331Y/D331Y
Time to descend the pole
12
9
6
3
0
1M
3M
6M
9M
12M
*
**
**
(F)
+Saline
+Levodopa
Distance (m)
80
60
40
20
0
**
#
PLA2G6WT/WT
PLA2G6WT/D331Y
PLA2G6D331Y/D331Y
(G)
+Saline
+Levodopa
Velocity (mm/s)
28
21
14
7
0
**
#
PLA2G6WT/WT
PLA2G6WT/D331Y
PLA2G6D331Y/D331Y

◀ **Fig. 4** PLA2G6$^{D331Y/D331Y}$ KI mice display early-onset motor deficits of parkinsonism. The velocity (**a**) and distance (**b**) of locomotor activity were progressively decreased in PLA2G6$^{D331Y/D331Y}$ mice at the age of 6 to 12 months. Age-matched heterozygous PLA2G6$^{WT/D331Y}$ mice did not exhibit the phenotype of hypoactivity. Ear bar represents the mean ± SEM of 20 mice. **c** Cylinder test was conducted to determine the spontaneous activity of animal. The motor deficit of 6- to 12-month-old homozygous PLA2G6$^{D331Y/D331Y}$ mice was indicated by a significant decrease in the number of rears. Each bar shows the mean ± SEM of 20 animals. **d** Rotarod test demonstrated that compared to age-matched WT or PLA2G6$^{WT/D331Y}$ mice, 6- to 12-month-old PLA2G6$^{D331Y/D331Y}$ KI mice displayed a marked reduction in the latency to fall. Each bar represents the mean ± SEM of 20 animals. **e** Pole test demonstrated that homozygous PLA2G6$^{D331Y/D331Y}$ mice at the age of 6 to 12 months displayed motor dysfunction by taking a longer time to execute the pole test. Each bar shows the mean ± SEM of 20 animals. Forty minutes after injecting saline or methyl L-DOPA (1.5 mg/kg of body weight) into animals, the distance (**f**) and velocity (**g**) of locomotion activity were analyzed. PLA2G6$^{D331Y/D331Y}$ mice injected with saline exhibited a reduced distance and velocity of locomotor activity. Following the administration of methyl L-DOPA, the hypoactivity displayed by 9-month-old PLA2G6$^{D331Y/D331Y}$ KI mice was improved, which was indicated by an increase in the locomotor activity (**f** and **g**). Each bar shows the mean ± SEM of 10 animals. $^{*}P < 0.05$, $^{**}P < 0.01$ compared to WT mice. $^{\#}P < 0.05$ compared to PLA2G6$^{D331Y/D331Y}$ mice injected with saline

determined by measuring the lipid peroxidation of mitochondria and the release of cytochrome c simultaneously [22].

Overproduction of mitochondrial ROS was observed in the SN of PLA2G6$^{D331Y/D331Y}$ mice (Fig. 5j). Lipid peroxidation of mitochondria was evaluated by performing thiobarbituric acid reactive substances assay. An increased level of lipid peroxidation was found in the SN of PLA2G6$^{D331Y/D331Y}$ mice (Fig. 5k). Cytosolic level of cytochrome c was also markedly upregulated in the SN of PLA2G6 $^{D331Y/D331Y}$ mice (Fig. 5l).

Homozygous (D331Y) PLA2G6 Mutation Causes the Activation of Mitochondrial Apoptotic Pathway, the Induction of Endoplasmic Reticulum Stress, and Mitophagy Dysfunction

To test the possibility that the activation of mitochondrial apoptotic pathway causes cell death of SN dopaminergic neurons observed in PLA2G6$^{D331Y/D331Y}$ mice, apoptotic proteins were evaluated in the SN of WT or KI mice. The level of cytosolic cytochrome c, active caspase-9, or active caspase-3 was significantly increased in the SN of PLA2G6$^{D331Y/D331Y}$ mice at the age of 9 months (Fig. 6a).

ER stress is implicated in the pathogenesis of PD [23]. Mitochondrial dysfunction results in overproduction of ROS, which then gives rise to ER stress [24, 25]. To determine whether homozygous (D331Y) PLA2G6 mutation triggers ER stress, protein levels of ER stress-related proteins were examined in the SN of WT or KI mice. Protein levels of 78-kDa glucose-regulated protein (Grp78), inositol-requiring enzyme 1α (IRE1α), protein kinase RNA-like ER kinase (PERK), and C/EBP homologous protein (CHOP), which participate in the activation of ER stress, were increased in the SN of PLA2G6$^{D331Y/D331Y}$ mice.

Impaired mitophagy plays an important role in the pathogenesis of PD [4]. Immunoblotting analysis demonstrated that protein levels of parkin and BNIP3, which are autophagy/mitophagy-related proteins [26, 27], were decreased in the SN of PLA2G6$^{D331Y/D331Y}$ knockin mice (Fig. 6c).

(D331Y) PLA2G6 Alters mRNA Levels of Genes, Which Possess Neurotoxic or Neuroprotective Effect, in the SN of PLA2G6$^{D331Y/D331Y}$ Knockin Mice

In addition to participating in maintaining mitochondrial function, PLA2G6 also participates in gene regulation [12]. Therefore, mutant (D331Y) PLA2G6-induced transcriptional dysregulation is also likely to be involved in (D331Y) PLA2G6-induced neuronal death of SNpc dopaminergic cells. To test this possibility, transcriptomic analysis was conducted to evaluate differential mRNA expressions in the SN of PLA2G6$^{D331Y/D331Y}$ mice at the age of 9 months. The heat map produced by hierarchical gene clustering displayed a different pattern between WT mice and PLA2G6$^{D331Y/D331Y}$ mice (Fig. 7a). We further investigated ten genes, which are involved in regulating neuronal death or survival (Table 1).

Microarray analysis indicated that the mRNA expression of microtubule affinity-regulating kinase 4 (Mark4), which causes neurotoxic effects [28], and XIAP associated factor 1 (Xaf1), which participates in the induction of apoptosis [29], was increased in the SN of PLA2G6$^{D331Y/D331Y}$ KI mouse. The mRNA expression of bone morphogenetic protein 6 (Bmp6), cyclin D2 (Ccnd2), beta-catenin 1 (Ctnnb1), heat shock protein 1B (Hspa1b), mitogen-activated protein kinase 1 (Mapk1), kinase D-interacting substrate 220 (Kidins220), prosaposin (Psap), and syndecan 2 (Sdc2), which exert a neuroprotective effect [30–37] was downregulated in the SN of PLA2G6$^{D331Y/D331Y}$ mice (Fig. 7a and Table 1).

Consistent with results of microarray analysis, quantitative RT-PCR analysis demonstrated that mRNA level of Mark4 or Xaf1 was significantly increased in the SN of PLA2G6$^{D331Y/D331Y}$ mice (Fig. 7b). The mRNA expression of Bmp6, Ccnd2, Ctnnb1, Hspa1b, Mapk1, Kidins220, Psap, and Sdc2 was downregulated in the SN of PLA2G6$^{D331Y/D331Y}$ mice (Fig. 7b).

To provide the evidence that prior to a significant neurodegeneration of SNpc dopaminergic cells, differential mRNA expression of these 10 genes is observed at the earlier phase of disease, WT or PLA2G6$^{D331Y/D331Y}$ mice at the age of 5 months, which did not exhibit a significant degeneration of SNpc dopaminergic cells, were used to conduct quantitative RT-PCR analysis. An upregulated mRNA level of Mark4 or Xaf1 and a downregulated mRNA level of Bmp6, Ccnd2,

Ctnnb1, Hspa1b, Mapk1, Kidins220, Psap, or Sdc2 were observed in the SN of PLA2G6$^{D331Y/D331Y}$ mice at the age of 5 months (Fig. 7c).

Consistent with the results of transcriptomic analysis and quantitative RT-PCR assays, western blot study demonstrated that protein expression of Mark4 or Xaf1 was upregulated in the SN of PLA2G6$^{D331Y/D331Y}$ mice at the age of 9 months (Fig. 7d, e). Protein expression of Bmp6, Ccnd2, Ctnnb1, Hspa1b, Mapk1, Kidins220, Psap, or Sdc2 was also downregulated in the SN of PLA2G6$^{D331Y/D331Y}$ mice (Fig. 7d, e).

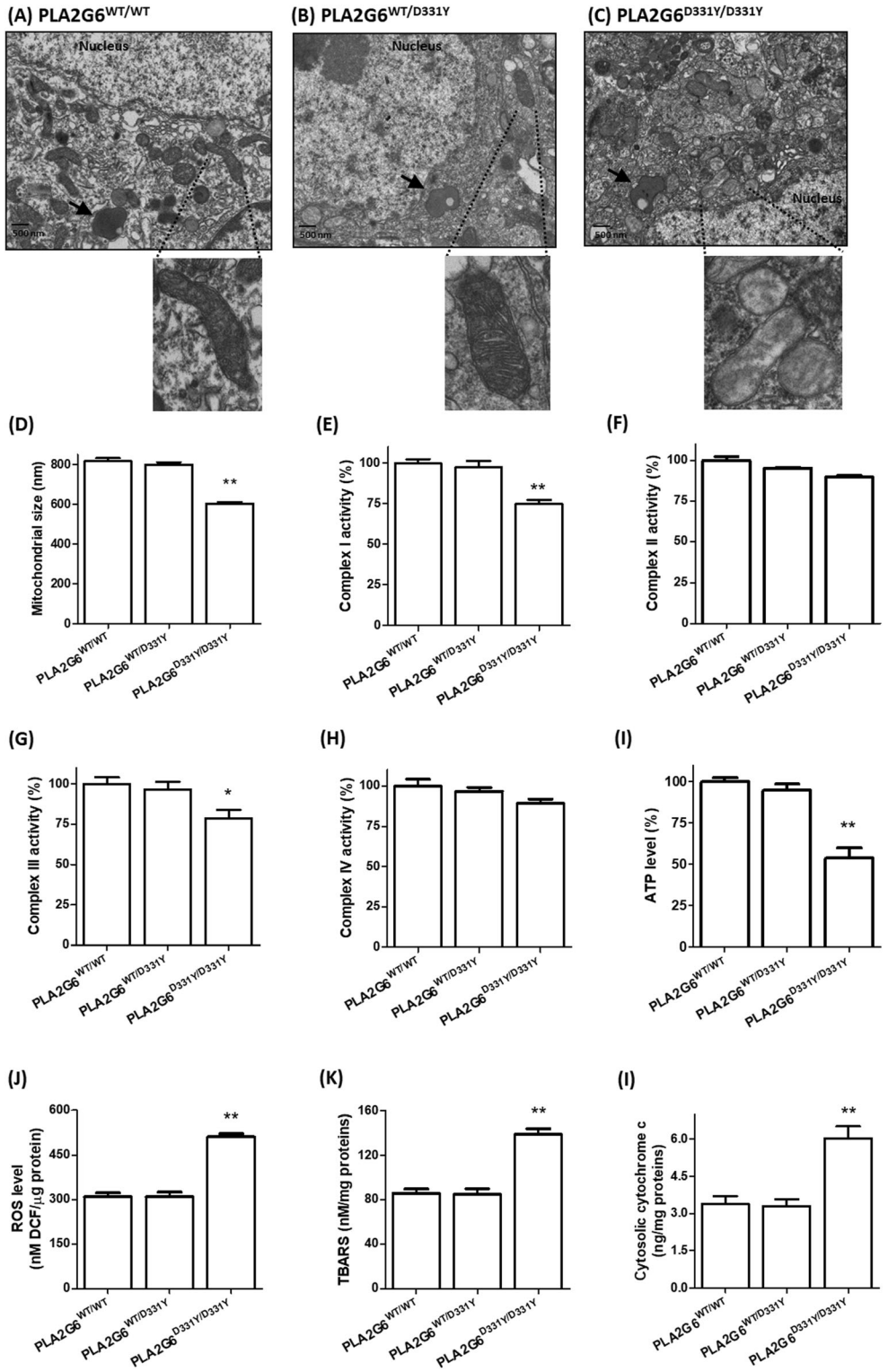

◀ **Fig. 5** Homozygous (D331Y) PLA2G6 mutation leads to abnormality in the ultrastructure of mitochondria and mitochondrial dysfunction. **a**–**c** In the neuromelanin-positive putative SNpc dopaminergic neurons of WT or PLA2G6$^{WT/D331Y}$ mice, mitochondrial morphology was intact, and mitochondrial cristae had a regular arrangement. In contrast, disrupted structure of mitochondria cristae was observed in the neuromelanin organelle-containing putative SNpc dopaminergic neurons of homozygous PLA2G6$^{D331Y/D331Y}$ mice. The arrow indicates neuromelanin organelle. **d** Compared to WT mice, the size of mitochondria was decreased in the SN of homozygous (D331Y) PLA2G6 mice. Each bar shows the mean ± SEM of 672–886 mitochondria. **e**–**h** The activity of mitochondrial complex I and III was significantly decreased in the SN of PLA2G6$^{D331Y/D331Y}$ KI mice as compared to WT mice. The activity of mitochondrial complex II or complex IV in the SN of homozygous (D331Y) PLA2G6 KI mice was not significantly different from that of WT mice. For mitochondrial complex I experiments, each bar represents the mean ± SEM of 20 mice. For mitochondrial complex II-IV experiments, each bar shows the mean ± SEM of 10 mice. The activity of mitochondrial complex was normalized with the activity of citrate synthase. **i** Intracellular ATP level was reduced in the SN of homozygous (D331Y) PLA2G6 KI mice. **j** Compared to WT or PLA2G6$^{WT/D331Y}$ mice, overproduction of ROS was observed in the SN of PLA2G6$^{D331Y/D331Y}$ KI mice. **k** The level of mitochondrial lipid peroxidation was upregulated in the SN of homozygous PLA2G6$^{D331Y/D331Y}$ mice. **l** Cytosolic level of cytochrome c was increased in the SN of PLA2G6$^{D331Y/D331Y}$ mice. $^{**}P < 0.01$ compared with wild-type mice. Each bar represents the mean ± SEM of 20 animals

Discussion

Mutations of PLA2G6 gene cause early-onset autosomal recessive PARK14 [38, 39]. A homozygous (D331Y) mutation of PLA2G6 has been reported to be the genetic cause of PARK14 [7–9]. Patients with homozygous (D331Y) PLA2G6 mutation exhibit motor dysfunctions of pure early-onset PD [7–9]. In the present study, homozygous PLA2G6$^{D331Y/D331Y}$ mice were prepared to investigate the pathogenic mechanism of (D331Y) PLA2G6-induced Parkinson's disease.

Consistent with previous neuropathological studies reporting degeneration of SNpc dopaminergic neurons in PARK14 patients [19, 40], PLA2G6$^{D331Y/D331Y}$ KI mice displayed early-onset neuronal death of SNpc dopaminergic cells at the age of 6 months. A decrease in striatal ^{18}F-FP-DTBZ uptake and a reduced level of striatal TH^{+}-staining observed in PLA2G6$^{D331Y/D331Y}$ mice at the age of 9 months indicated the degeneration of nigrostriatal dopaminergic terminals caused by homozygous (D331Y) PLA2G6 mutation. Consistent with our finding showing that 6- or 9-month-old PLA2G6$^{D331Y/D331Y}$ mice exhibited degeneration of SNpc dopaminergic neurons, PLA2G6$^{D331Y/D331Y}$ KI mice at the age of 6 or 9 months displayed early-onset PD phenotypes including slowness of movement, hypoactivity, and impaired motor performance. In accordance with previous studies reporting that L-DOPA is effective in treating PD patients with (D331Y) PLA2G6 mutation [7–9], the hypoactivity displayed by 9-month-old PLA2G6$^{D331Y/D331Y}$ mice was reversed by the treatment of L-DOPA. Previous studies demonstrated the presence of Lewy bodies in the brain of PARK 14 patients [19, 40], our results indicated that Lewy bodies were also found in the SN of PLA2G6$^{D331Y/D331Y}$ KI mice at the age of 9 months. Aggregation of hyperphosphorylated tau, which is characteristics of tau pathology, was found in the brain of PARK14 patients [19]. In our study, upregulated protein level of phospho-tau$^{Ser202/Thr205}$ was observed in the SN of homozygous PLA2G6$^{D331Y/D331Y}$ mice at the age of 9 months.

PLA2G6 knockout (KO) mice have been used to investigate PLA2G6 deficiency-induced pathological effects. PLA2G6 KO mice at the age of 14 months exhibit motor deficits and the loss of dopaminergic nerve terminal in the striatum [41]. Fourteen-month-old PLA2G6 KO mice do not display a significant cell death of SNpc dopaminergic neurons [41]. PLA2G6 KO mice at the age of 12 months exhibit the degeneration of mitochondrial inner membrane and presynaptic membranes/axon [42]. The expression of αSyn is increased in 12-month-old PLA2G6 KO mice [43, 44]. The formation of p-αSyn-positive granules is found in PLA2G6 KO mice at the age of 12 months [44]. Compared to PLA2G6 KO mouse model, PLA2G6$^{D331Y/D331Y}$ KI mice at the age of 6 or 9 months prepared by us display early-onset parkinsonism phenotypes, the formation of Lewy body, and early-onset cell death of SNpc dopaminergic neurons. Therefore, we, for the first time, prepared a successful knockin mouse model of early-onset PARK14.

PARK14 (D331Y) mutation has been shown to cause the loss of function of PLA2G6 [8]. In this study, homozygous PLA2G6$^{D331Y/D331Y}$ mice also displayed impaired activity of PLA2G6 in the SN. Deficiency of PLA2G6 has been shown to cause abnormality in the morphology and function of mitochondria in the fly model [13]. It is very likely that homozygous (D331Y) PLA2G6 mutation leads to an abnormal ultrastructure of mitochondria in SNpc dopaminergic cells. In accordance with this hypothesis, disrupted cristae of mitochondria were found in SN dopaminergic neurons of PLA2G6 $^{D331Y/D331Y}$ KI mice.

Mitochondrial dysfunction participates in the etiology of SNpc dopaminergic neuronal death observed in Parkinson's disease [45]. Mitochondrial structural abnormality found in the SN dopaminergic cells of PLA2G6$^{D331Y/D331Y}$ knockin mice is expected to cause the mitochondrial dysfunction. In accordance with this hypothesis, decreased complex I activity or ATP level and increased ROS production were found in the substantia nigra of homozygous PLA2G6$^{D331Y/D331Y}$ mice. Our study further suggests that overproduction of ROS resulting from mitochondrial dysfunction induces the apoptosis of SN dopaminergic neurons of PLA2G6$^{D331Y/D331Y}$ mice by causing the oxidation of cardiolipin and the release of cytochrome c, resulting in the upregulated expression of active caspase-9 and active caspase-3.

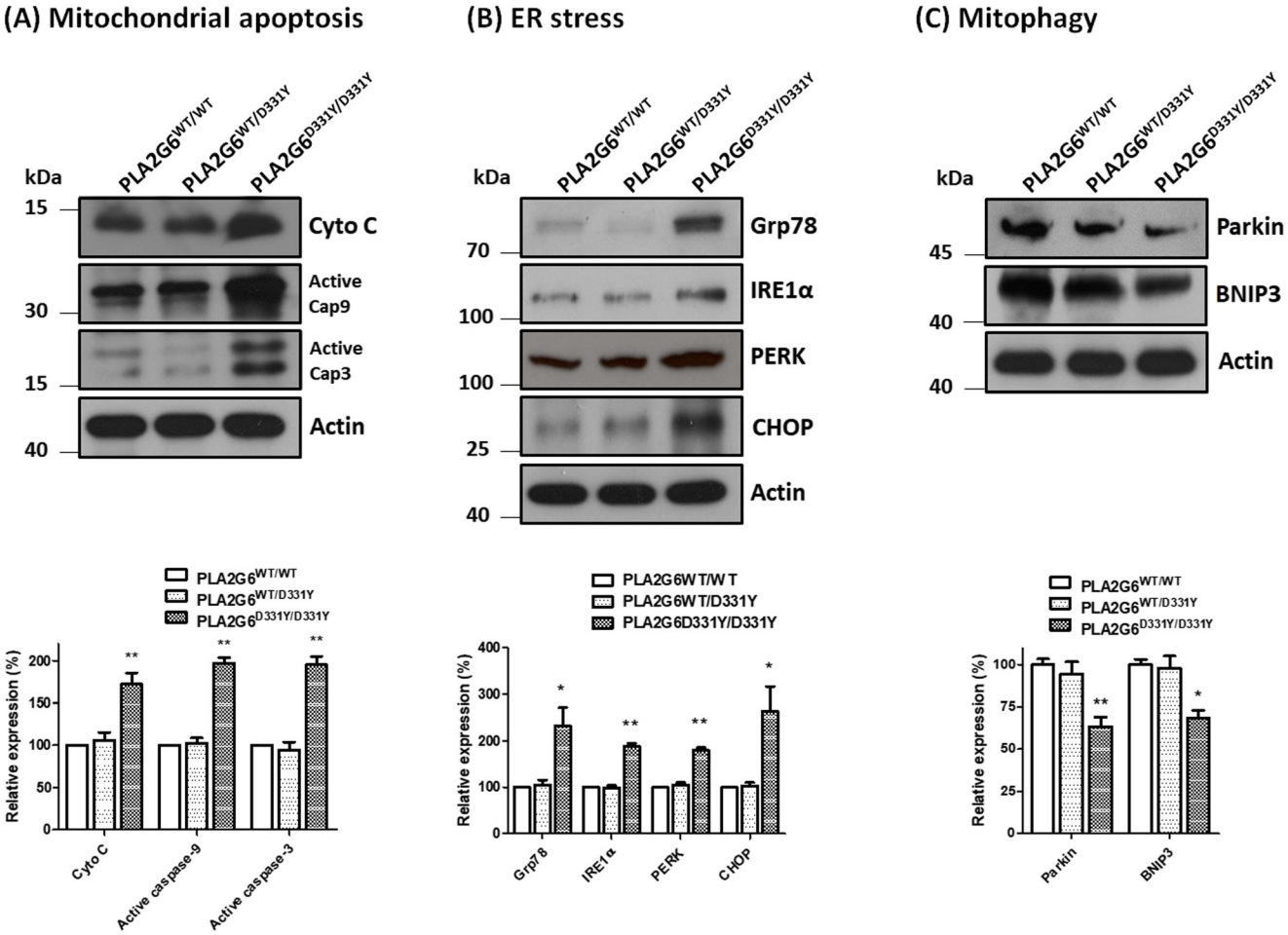

Fig. 6 Homozygous (D331Y) PLA2G6 mutation causes activation of mitochondria apoptotic cascade, induction of ER stress, and mitophagy dysfunction. **a** Western blot analysis showed that protein expression of active caspase-3, active caspase-9, or cytochrome c (Cyto c) in the cytosol was upregulated in the SN of homozygous (D331Y) PLA2G6 KI mice at the age of 9 months. **b** Protein levels of Grp78, IRE1, PERK, and CHOP were increased in the substantia nigra of PLA2G6$^{D331Y/D331Y}$ knockin mice. **c** Immunoblotting analysis showed that protein expression of parkin or BNIP3 was significantly downregulated in the SN of PLA2G6$^{D331Y/D331Y}$ KI mice. $^{*}P < 0.05$, $^{**}P < 0.01$ compared with WT mice. Each bar shows the mean ± SEM of five experiments

In the present study, overproduction of mitochondrial ROS, oxidative stress, and α-synuclein aggregations were observed in the SN of PLA2G6$^{D331Y/D331Y}$ mice. Upregulated level of ROS and oxidative stress are believed to cause the accumulation and aggregation of α-synuclein [46]. Production of ROS upregulates the level of casein kinase 2, which participates in ROS-dependent α-synuclein aggregation by phosphorylating α-synuclein at Ser129 [47]. Therefore, it is possible that overproduction of ROS and oxidative stress may cause α-synuclein aggregation in the SN of PLA2G6$^{D331Y/D331Y}$ KI mice.

ER is responsible for protein folding and protein modification. Neuronal cells are susceptible to misfolded and aggregated proteins. The accumulation of misfolded protein causes chronic ER stress and induces unfolded protein response (UPR), which protects neurons against intracellular misfolded proteins. Glucose-regulated protein 78 (Grp78) is an important regulator of the UPR. Grp78 binds to misfolded proteins and activates downstream sensor proteins of UPR, which are inositol-requiring 1α (IRE-1α), activating transcription factor 6 (ATF6), and protein kinase RNA-like endoplasmic reticulum kinase (PERK) [48]. However, under prolonged ER stress, deleterious UPR signaling stimulates the activation of C/EBP homologous protein (CHOP) and triggers apoptotic neuronal death [49]. ER stress is believed to induce apoptosis of SNpc dopaminergic neurons and is involved in the etiology of Parkinson's disease [23]. Overproduction of ROS resulting from mitochondrial dysfunction causes ER stress [24, 25]. Accumulation of α-synuclein triggers ER stress-mediated apoptotic neuronal death [50]. In the present study, increased ROS generation and upregulated protein expression of α-synuclein were found in the SN of PLA2G6$^{D331Y/D331Y}$ KI mouse, suggesting that ER stress is involved in homozygous (D331) PLA2G6 mutation-induced neurodegeneration of SNpc dopaminergic cells. In accordance with this hypothesis, upregulated protein levels of Grp78, IRE1α, PERK, and

CHOP, which participate in the activation of ER stress, were found in the SN of PLA2G6$^{D331Y/D331Y}$ KI mice.

Autophagy is a crucial process responsible for the removal of aggregated proteins or damaged organelles. Mitophagy, a selective autophagic degradation of mitochondria, eliminates dysfunctional mitochondria through autophagy machinery and maintains mitochondrial turnover and functionality [51]. The impairment of autophagy/mitophagy results in the loss of

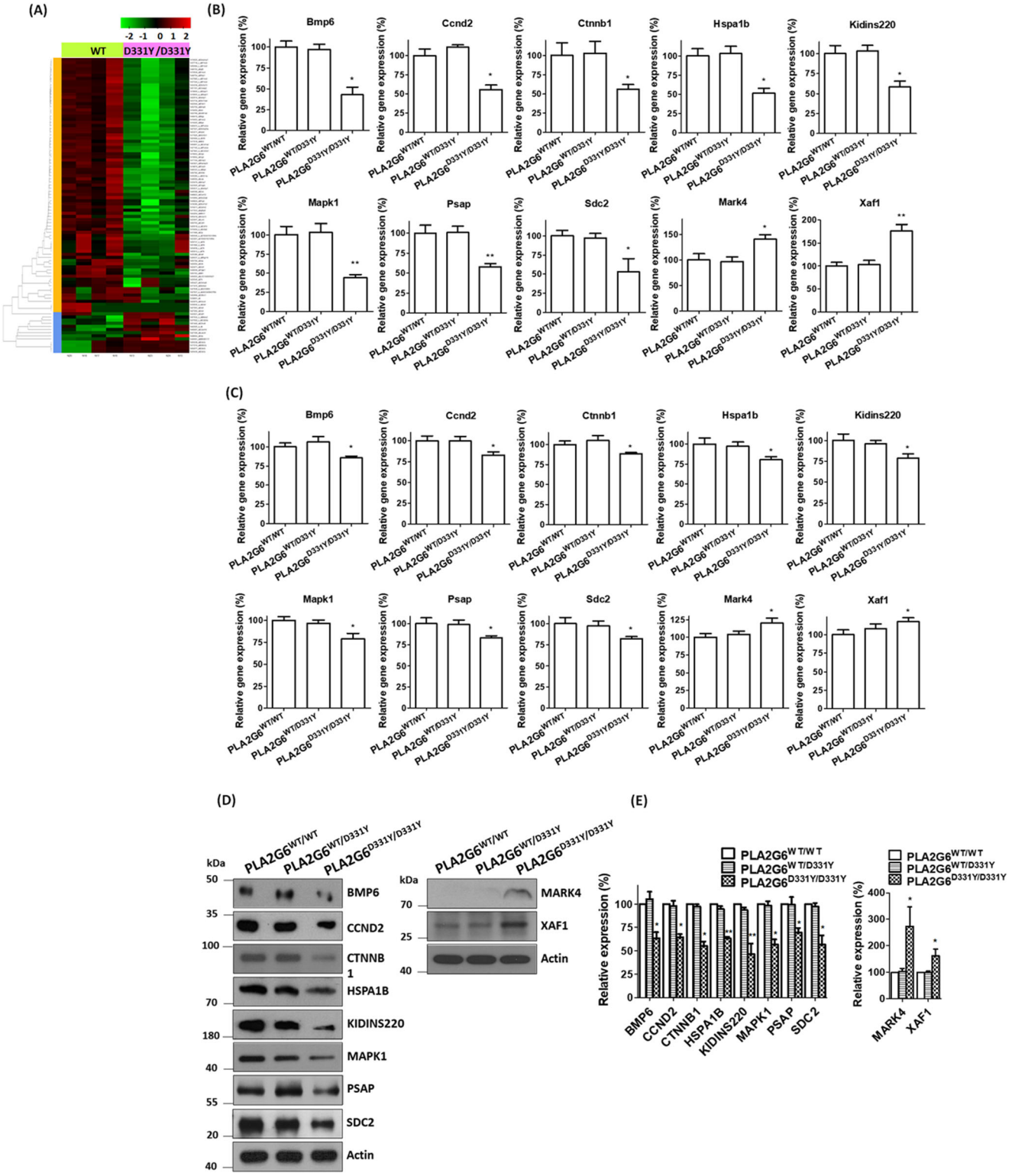

◀ **Fig. 7** Homozygous (D331Y) PLA2G6 KI mice display differential gene expressions. **a** Heat maps with hierarchical clustering revealed dramatic gene dysregulation in the substantia nigra of PLA2G6$^{D331Y/D331Y}$ KI mice at the age of 9 months compared with WT mice at the same age. **b** Quantitative real-time PCR analysis was performed to validate selected ten genes. The mRNA levels of Bmp6, Ccnd2, Ctnnb1, Hspa1b, Kidin220, Mapk1, Psap, and Sdc2 were decreased in the substantia nigra of PLA2G6$^{D331Y/D331Y}$ mice at the age of 9 months. The mRNA expression of Mark4 or Xaf1 was upregulated in the SN of PLA2G6$^{D331Y/D331Y}$ KI mice. Each bar represents the mean ± SEM of four experiments. **c** Compared to WT mice, mRNA levels of eight genes (Bmp6, Ccnd2, Hspa1b, Kidin220, Mapk1, Psap, and Sdc2) were decreased in the SN of 5-month-old PLA2G6$^{D331Y/D331Y}$ mice. The mRNA expression of Mark4 or Xaf1 was upregulated in the substantia nigra of PLA2G6$^{D331Y/D331Y}$ mice at the age of 5 months. Each bar shows the mean ± SEM of four independent experiments. **d**, **e** Protein levels of BMP6, CCND2, CTNNB1, HSPA1B, KIDINS220, MAPK1, PSAP, and SDC2 were decreased in the substantia nigra of PLA2G6$^{D331Y/D331Y}$ mice. Protein levels of MARK4 and XAF1 were increased in the substantia nigra of homozygous (D331Y) PLA2G6 mice at the age of 9 months. *$P < 0.05$, **$P < 0.01$ compared with wild-type mice. Each bar shows the mean ± SEM of four experiments

SN dopaminergic neurons and is involved in the etiology of Parkinson's disease [51]. In this study, protein levels of mitophagic proteins, including parkin and BNIP3 [26, 27], were decreased in the SN of homozygous PLA2G6$^{D331Y/D331Y}$ mice. This finding suggests the possible involvement of mitophagy dysfunction in (D331Y) PLA2G6 mutation-induced neurodegeneration of SNpc dopaminergic cells.

PLA2G6 has been shown to regulate gene expression [12]. Therefore, (D331Y) PLA2G6-induced transcriptional abnormality could be involved in (D331Y) PLA2G6-induced degeneration of SNpc dopaminergic neurons. Downregulation of neuroprotective pathways and upregulation of neurotoxic signaling could lead to neuronal death of SNpc dopaminergic cells. The results of this study showed that mRNA levels of Bmp6, Ccnd2, Ctnnb1, Hspa1b, Kidins220, Mapk1, Psap, and Sdc2, which are involved in neuroprotective signaling, neurogenesis, or neuronal survival, were decreased in the SN of PLA2G6$^{D331Y/D331Y}$ mice. Bmp6 is a member of the transforming growth factor β superfamily and processes neuroprotective effect against oxidative stress [33]. Bmp6 also promotes neurite outgrowth, neurogenesis, and neuronal survival [52]. Moreover, Bmp6 functions a neurotrophic factor by augmenting dopamine uptake in primary cultured dopaminergic neurons [53]. Ccnd2 is involved in promoting neurogenesis and neuronal differentiation [54]. Ctnnb1 participates in the development and maintenance of dopaminergic cells [55]. Loss of Ctnnb1 leads to downregulation of progenitor genes in midbrain dopaminergic neurons [56]. Nigrostriatal dopaminergic neurons of Hspa1b knockout mice are more sensitive to MPTP-induced neurotoxic effect [37]. A high level of Kidins220 expression is observed in the nervous system. Kidins220 functions as a mediator of several signaling pathways, which are required for neuronal survival and differentiation [57]. Kidins220 also modulates synaptic transmission and plasticity [58]. Mapk1 is believed to be essential for neuronal survival and function of dopaminergic cells [32]. Psap acts as a neurotrophic factor and exerts a neuroprotective effect [36]. Psap protein secreted by bone marrow stromal cell-derived neuroprogenitor cells prevents apoptotic neuronal death [59]. Psap-derived 18-mer peptide inhibits apoptosis of SN dopaminergic cells observed in MPTP-induced mouse model of PD [60]. Sdc2 plays a role in dendritic spine morphogenesis of hippocampal neurons and regulates neurite outgrowth [31].

In this study, mRNA levels of Mark4 and Xaf1, which participate in the activation of apoptotic pathway, were increased in the SN of homozygous PLA2G6$^{D331Y/D331Y}$ mice. Mark4 decreases cell viability and is a positive regulator of apoptosis [61]. X-linked inhibitor of apoptosis (XIAP) is an important apoptotic regulator during neuronal apoptosis [62]. Xaf1, an antagonist of XIAP, directly binds to XIAP and triggers apoptotic death by inhibiting anti-caspase activity of XIAP [29].

If downregulated mRNA level of Bmp6, Ccnd2, Ctnnb1, Hspa1b, Kidins220, Mapk1, Psap, or Sdc2 and upregulated mRNA level of Mark4 or Xaf1 participate in the etiology of (D331Y) PLA2G6-induced neuronal death of SN

Table 1 Altered mRNA expressions in the SN of homozygous (D331Y) PLA2G6 KI mice

Gene	Gene symbol	Fold change
XIAP associated factor 1	Xaf1	5.991
MAP/microtubule affinity-regulating kinase 4	Mark4	1.913
Heat shock protein 1B	Hspa1b	− 4.327
Syndecan 2	Sdc2	− 3.369
Kinase D-interacting substrate 220	Kidins220	− 3.266
Catenin (cadherin associated protein), beta 1	Ctnnb1	− 3.072
Mitogen-activated protein kinase 1	Mapk1	− 3.003
Prosaposin	Psap	− 2.638
Bone morphogenetic protein 6	Bmp6	− 2.635
Cyclin D2	Ccnd2	− 2.137

dopaminergic cells observed in PLA2G6$^{D331Y/D331Y}$ KI mice at the age of 9 months, differential mRNA expressions of these 10 genes should be observed in homozygous (D331Y) PLA2G6 mouse at the earlier phase of disease. In this study, PLA2G6$^{D331Y/D331Y}$ KI mouse at the age of 5 months did not display a significant degeneration of SNpc dopaminergic neurons. However, altered mRNA levels of these 10 genes were found in PLA2G6$^{D331Y/D331Y}$ mice at the age of 5 months.

In summary, we, for the first time, generated knockin mouse model of PARK14 (D331Y) PLA2G6-induced Parkinson's disease by preparing PLA2G6$^{D331Y/D331Y}$ KI mice. PLA2G6$^{D331Y/D331Y}$ mice exhibited early-onset neurodegeneration of SNpc dopaminergic cells and PD phenotypes. The results of our study suggest that homozygous (D331Y) PLA2G6 mutation induces neuronal death of SNpc dopaminergic cells by causing mitochondrial dysfunction, elevated ER stress, mitophagy impairment, and transcriptional abnormality.

Acknowledgements The authors are grateful to Microscopy Core Laboratory and Center for Advanced Molecular Imaging and Translation, Department of Nuclear Medicine, Chang Gung Memorial Hospital, Linkou, Taoyuan, Taiwan. We thank Han Chiu and Chia-Chen Hsu for assistance and technical support. We would like to thank Chih-Wei Hu and Wen-Ai Wu of Transgenic Mouse Core Laboratory of Experimental Animal Center for help with ES cells microinjection.

Funding Information This work was supported by the Ministry of Science and Technology, Taiwan (MOST 104-2314-B-182A-35-, MOST 105-2314-B-038-092-MY3 and MOST 105-2314-B-182A-013-MY3 to TH Yeh; MOST 105-2314-B-182A-003- and MOST 106-2314-B-182A-012-MY3 to CC Chiu; MOST104-2320-B-182-014-MY3 to HL Wang), Taipei Medical University (TMU106-AE1-B20 to TH Yeh), and the Chang Gung Medical Foundation (grants CMRPG3C1482, CMRPG3C0783, CMRPG3C1491, CMRPG3C1492, CMRPG3D0382, CRRPG3C0023, CRRPG3C0033 to TH Yeh.; CMRPG3F1821 to CC Chiu; CMRPD1B0332, CMRPD1C0623, CRRPD1C0013, CMRPD180433, and EMRPD1F0251 to HL Wang).

Compliance with Ethical Standards

Animal experiments were performed in accordance with protocols approved by Institutional Animal Care and Use Committee (IACUC) of Chang Gung University.

Conflict of Interest The authors declare that they have no competing financial interests.

References

1. Dickson DW, Braak H, Duda JE, Duyckaerts C, Gasser T, Halliday GM, Hardy J, Leverenz JB et al (2009) Neuropathological assessment of Parkinson's disease: Refining the diagnostic criteria. Lancet Neurol 8(12):1150–1157. https://doi.org/10.1016/S1474-4422(09)70238-8S1474-4422(09)70238-8
2. Spillantini MG, Crowther RA, Jakes R, Hasegawa M, Goedert M (1998) alpha-Synuclein in filamentous inclusions of Lewy bodies from Parkinson's disease and dementia with Lewy bodies. Proc Natl Acad Sci U S A 95(11):6469–6473
3. Schapira AH, Jenner P (2011) Etiology and pathogenesis of Parkinson's disease. Mov Disord 26(6):1049–1055. https://doi.org/10.1002/mds.23732
4. Menzies FM, Fleming A, Caricasole A, Bento CF, Andrews SP, Ashkenazi A, Fullgrabe J, Jackson A et al (2017) Autophagy and neurodegeneration: pathogenic mechanisms and therapeutic opportunities. Neuron 93(5):1015–1034. https://doi.org/10.1016/j.neuron.2017.01.022
5. Houlden H, Singleton AB (2012) The genetics and neuropathology of Parkinson's disease. Acta Neuropathol 124(3):325–338. https://doi.org/10.1007/s00401-012-1013-5
6. Hayflick SJ, Kurian MA, Hogarth P (2018) Neurodegeneration with brain iron accumulation. Handb Clin Neurol 147:293–305. https://doi.org/10.1016/B978-0-444-63233-3.00019-1
7. Lu CS, SC Lai RMW, Weng YH, Huang CL, Chen RS, Chang HC, Wu-Chou YH, Yeh TH (2012) PLA2G6 mutations in PARK14-linked young-onset parkinsonism and sporadic Parkinson's disease. Am J Med Genet B Neuropsychiatr Genet 159B(2):183–191. https://doi.org/10.1002/ajmg.b.32012
8. Shi CH, Tang BS, Wang L, Lv ZY, Wang J, Luo LZ, Shen L, Jiang H et al (2011) PLA2G6 gene mutation in autosomal recessive early-onset parkinsonism in a Chinese cohort. Neurology 77(1):75–81
9. Xie F, Cen Z, Ouyang Z, Wu S, Xiao J, Luo W (2015) Homozygous p.D331Y mutation in PLA2G6 in two patients with pure autosomal-recessive early-onset parkinsonism: further evidence of a fourth phenotype of PLA2G6-associated neurodegeneration. Parkinsonism Relat Disord 21(4):420–422. https://doi.org/10.1016/j.parkreldis.2015.01.012S1353-8020(15)00032-2
10. Ramanadham S, Ali T, Ashley JW, Bone RN, Hancock WD, Lei X (2015) Calcium-independent phospholipases A2 and their roles in biological processes and diseases. J Lipid Res 56(9):1643–1668. https://doi.org/10.1194/jlr.R058701jlr.R058701
11. Ong WY, Farooqui T, Farooqui AA (2010) Involvement of cytosolic phospholipase A(2), calcium independent phospholipase A(2) and plasmalogen selective phospholipase A(2) in neurodegenerative and neuropsychiatric conditions. Curr Med Chem 17(25):2746–2763
12. Xie Z, MC Gong WS, Turk J, Guo Z (2007) Group VIA phospholipase A2 (iPLA2beta) participates in angiotensin II-induced transcriptional up-regulation of regulator of g-protein signaling-2 in vascular smooth muscle cells. J Biol Chem 282(35):25278–25289. https://doi.org/10.1074/jbc.M611206200
13. Kinghorn KJ, Castillo-Quan JI, Bartolome F, Angelova PR, Li L, Pope S, Cocheme HM, Khan S et al (2015) Loss of PLA2G6 leads to elevated mitochondrial lipid peroxidation and mitochondrial dysfunction. Brain 138(Pt 7):1801–1816. https://doi.org/10.1093/brain/awv132awv132
14. Beck G, Sugiura Y, Shinzawa K, Kato S, Setou M, Tsujimoto Y, Sakoda S, Sumi-Akamaru H (2011) Neuroaxonal dystrophy in calcium-independent phospholipase A2beta deficiency results from insufficient remodeling and degeneration of mitochondrial and presynaptic membranes. J Neurosci 31(31):11411–11420. https://doi.org/10.1523/JNEUROSCI.0345-11.201131/31/11411
15. Zhou Q, Yen A, Rymarczyk G, Asai H, Trengrove C, Aziz N, Kirber MT, Mostoslavsky G et al (2016) Impairment of PARK14-dependent Ca(2+) signalling is a novel determinant of Parkinson's disease. Nat Commun 7:10332. https://doi.org/10.1038/ncomms10332ncomms10332
16. Gao L, Hidalgo-Figueroa M, Escudero LM, Diaz-Martin J, Lopez-Barneo J, Pascual A (2013) Age-mediated transcriptomic changes in adult mouse substantia nigra. PLoS One 8(4):e62456. https://doi.org/10.1371/journal.pone.0062456
17. Masuda-Suzukake M, Nonaka T, Hosokawa M, Oikawa T, Arai T, Akiyama H, Mann DM, Hasegawa M (2013) Prion-like spreading

of pathological alpha-synuclein in brain. Brain 136(Pt 4):1128–1138. https://doi.org/10.1093/brain/awt037
18. Henderson MX, Chung CH, Riddle DM, Zhang B, Gathagan RJ, Seeholzer SH, Trojanowski JQ, Lee VMY (2017) Unbiased proteomics of early Lewy body formation model implicates active microtubule affinity-regulating kinases (MARKs) in synucleinopathies. J Neurosci 37(24):5870–5884. https://doi.org/10.1523/JNEUROSCI.2705-16.2017
19. Paisan-Ruiz C, Li A, Schneider SA, Holton JL, Johnson R, Kidd D, Chataway J, Bhatia KP et al (2012) Widespread Lewy body and tau accumulation in childhood and adult onset dystonia-parkinsonism cases with PLA2G6 mutations. Neurobiol Aging 33(4):814–823. https://doi.org/10.1016/j.neurobiolaging.2010.05.009S0197-4580(10)00223-X
20. Paisan-Ruiz C, Bhatia KP, Li A, Hernandez D, Davis M, Wood NW, Hardy J, Houlden H et al (2009) Characterization of PLA2G6 as a locus for dystonia-parkinsonism. Ann Neurol 65(1):19–23. https://doi.org/10.1002/ana.21415
21. Schapira AH, Cooper JM, Dexter D, Clark JB, Jenner P, Marsden CD (1990) Mitochondrial complex I deficiency in Parkinson's disease. J Neurochem 54(3):823–827
22. Kagan VE, Tyurin VA, Jiang J, Tyurina YY, Ritov VB, Amoscato AA, Osipov AN, Belikova NA et al (2005) Cytochrome c acts as a cardiolipin oxygenase required for release of proapoptotic factors. Nat Chem Biol 1(4):223–232. https://doi.org/10.1038/nchembio727
23. Remondelli P, Renna M (2017) The endoplasmic reticulum unfolded protein response in neurodegenerative disorders and its potential therapeutic significance. Front Mol Neurosci 10:187. https://doi.org/10.3389/fnmol.2017.00187
24. Celardo I, Costa AC, Lehmann S, Jones C, Wood N, Mencacci NE, Mallucci GR, Loh SH et al (2016) Mitofusin-mediated ER stress triggers neurodegeneration in pink1/parkin models of Parkinson's disease. Cell Death Dis 7(6):e2271. https://doi.org/10.1038/cddis.2016.173cddis2016173
25. Lei X, Zhang S, Bohrer A, Bao S, Song H, Ramanadham S (2007) The group VIA calcium-independent phospholipase A2 participates in ER stress-induced INS-1 insulinoma cell apoptosis by promoting ceramide generation via hydrolysis of sphingomyelins by neutral sphingomyelinase. Biochemistry 46(35):10170–10185. https://doi.org/10.1021/bi700017z
26. Rodolfo C, Campello S, Cecconi F (2017) Mitophagy in neurodegenerative diseases. Neurochem Int. https://doi.org/10.1016/j.neuint.2017.08.004
27. Thomas RL, Kubli DA, Gustafsson AB (2011) Bnip3-mediated defects in oxidative phosphorylation promote mitophagy. Autophagy 7(7):775–777
28. Yu W, Polepalli J, Wagh D, Rajadas J, Malenka R, Lu B (2012) A critical role for the PAR-1/MARK-tau axis in mediating the toxic effects of Abeta on synapses and dendritic spines. Hum Mol Genet 21(6):1384–1390. https://doi.org/10.1093/hmg/ddr576ddr576
29. Liston P, Fong WG, Kelly NL, Toji S, Miyazaki T, Conte D, Tamai K, Craig CG et al (2001) Identification of XAF1 as an antagonist of XIAP anti-caspase activity. Nat Cell Biol 3(2):128–133. https://doi.org/10.1038/35055027
30. Kowalczyk A, RK Filipkowski MR, Wilczynski GM, FA Konopacki JJ, Ciemerych MA, Sicinski P, Kaczmarek L (2004) The critical role of cyclin D2 in adult neurogenesis. J Cell Biol 167(2):209–213. https://doi.org/10.1083/jcb.200404181
31. IM Ethell FI, Kalo MS, Couchman JR, Pasquale EB, Yamaguchi Y (2001) EphB/syndecan-2 signaling in dendritic spine morphogenesis. Neuron 31(6):1001–1013
32. Cavanaugh JE, Jaumotte JD, Lakoski JM, Zigmond MJ (2006) Neuroprotective role of ERK1/2 and ERK5 in a dopaminergic cell line under basal conditions and in response to oxidative stress. J Neurosci Res 84(6):1367–1375. https://doi.org/10.1002/jnr.21024
33. Du J, Zhu Y, Chen X, Fei Z, Yang S, Yuan W, Zhang J, Zhu T (2007) Protective effect of bone morphogenetic protein-6 on neurons from H_2O_2 injury. Brain Res 1163:10–20. https://doi.org/10.1016/j.brainres.2007.06.002
34. Liu Y, Hao S, Yang B, Fan Y, Qin X, Chen Y, Hu J (2017) Wnt/beta-catenin signaling plays an essential role in alpha7 nicotinic receptor-mediated neuroprotection of dopaminergic neurons in a mouse Parkinson's disease model. Biochem Pharmacol 140:115–123. https://doi.org/10.1016/j.bcp.2017.05.017
35. Duffy AM, Schaner MJ, Wu SH, Staniszewski A, Kumar A, Arevalo JC, Arancio O, Chao MV et al (2011) A selective role for ARMS/Kidins220 scaffold protein in spatial memory and trophic support of entorhinal and frontal cortical neurons. Exp Neurol 229(2):409–420. https://doi.org/10.1016/j.expneurol.2011.03.008S0014-4886(11)00091-4
36. Meyer RC, Giddens MM, Coleman BM, Hall RA (2014) The protective role of prosaposin and its receptors in the nervous system. Brain Res 1585:1–12. https://doi.org/10.1016/j.brainres.2014.08.022S0006-8993(14)01086-5
37. Park HK, Cho AR, Lee SC, Ban JY (2012) MPTP-induced model of Parkinson's disease in heat shock protein 70.1 knockout mice. Mol Med Rep 5(6):1465–1468. https://doi.org/10.3892/mmr.2012.839
38. Yoshino H, Tomiyama H, Tachibana N, Ogaki K, Li Y, Funayama M, Hashimoto T, Takashima S et al (2010) Phenotypic spectrum of patients with PLA2G6 mutation and PARK14-linked parkinsonism. Neurology 75(15):1356–1361. https://doi.org/10.1212/WNL.0b013e3181f7364975/15/1356
39. Bonifati V (2014) Genetics of Parkinson's disease—state of the art, 2013. Parkinsonism Relat Disord 20(Suppl 1):S23–S28. https://doi.org/10.1016/S1353-8020(13)70009-9S1353-8020(13)70009-9
40. Miki Y, Yoshizawa T, Morohashi S, Seino Y, Kijima H, Shoji M, Mori A, Yamashita C et al (2017) Neuropathology of PARK14 is identical to idiopathic Parkinson's disease. Mov Disord 32(5):799–800. https://doi.org/10.1002/mds.26952
41. Beck G, Shinzawa K, Hayakawa H, Baba K, Sumi-Akamaru H, Tsujimoto Y, Mochizuki H (2016) Progressive axonal degeneration of nigrostriatal dopaminergic neurons in calcium-independent phospholipase A2beta knockout mice. PLoS One 11(4):e0153789. https://doi.org/10.1371/journal.pone.0153789
42. Sumi-Akamaru H, Beck G, Kato S, Mochizuki H (2015) Neuroaxonal dystrophy in PLA2G6 knockout mice. Neuropathology 35(3):289–302. https://doi.org/10.1111/neup.12202
43. Blanchard H, Taha AY, Cheon Y, Kim HW, Turk J, Rapoport SI (2014) iPLA2beta knockout mouse, a genetic model for progressive human motor disorders, develops age-related neuropathology. Neurochem Res 39(8):1522–1532. https://doi.org/10.1007/s11064-014-1342-y
44. Sumi-Akamaru H, Beck G, Shinzawa K, Kato S, Riku Y, Yoshida M, Fujimura H, Tsujimoto Y et al (2016) High expression of alpha-synuclein in damaged mitochondria with PLA2G6 dysfunction. Acta Neuropathol Commun 4:27. https://doi.org/10.1186/s40478-016-0298-3
45. Michel PP, Hirsch EC, Hunot S (2016) Understanding dopaminergic cell death pathways in Parkinson disease. Neuron 90(4):675–691. https://doi.org/10.1016/j.neuron.2016.03.038S0896-6273(16)30058-7
46. Esteves AR, Arduino DM, Silva DF, Oliveira CR, Cardoso SM (2011) Mitochondrial dysfunction: the road to alpha-synuclein oligomerization in PD. Parkinsons Dis 2011(693761):1–20. https://doi.org/10.4061/2011/693761
47. Takahashi M, Ko LW, Kulathingal J, Jiang P, Sevlever D, Yen SH (2007) Oxidative stress-induced phosphorylation, degradation and aggregation of alpha-synuclein are linked to upregulated CK2 and

cathepsin D. Eur J Neurosci 26(4):863–874. https://doi.org/10.1111/j.1460-9568.2007.05736.x

48. Mercado G, Castillo V, Vidal R, Hetz C (2015) ER proteostasis disturbances in Parkinson's disease: novel insights. Front Aging Neurosci 7:39. https://doi.org/10.3389/fnagi.2015.00039
49. Urra H, Dufey E, Lisbona F, Rojas-Rivera D, Hetz C (2013) When ER stress reaches a dead end. Biochim Biophys Acta 1833(12):3507–3517. https://doi.org/10.1016/j.bbamcr.2013.07.024S0167-4889(13)00311-X
50. Colla E, Coune P, Liu Y, Pletnikova O, Troncoso JC, Iwatsubo T, Schneider BL, Lee MK (2012) Endoplasmic reticulum stress is important for the manifestations of alpha-synucleinopathy in vivo. J Neurosci 32(10):3306–3320. https://doi.org/10.1523/JNEUROSCI.5367-11.201232/10/3306
51. Martinez-Vicente M (2017) Neuronal mitophagy in neurodegenerative diseases. Front Mol Neurosci 10:64. https://doi.org/10.3389/fnmol.2017.00064
52. Crews L, Adame A, Patrick C, Delaney A, Pham E, Rockenstein E, Hansen L, Masliah E (2010) Increased BMP6 levels in the brains of Alzheimer's disease patients and APP transgenic mice are accompanied by impaired neurogenesis. J Neurosci 30(37):12252–12262. https://doi.org/10.1523/JNEUROSCI.1305-10.201030/37/12252
53. Jordan J, Bottner M, Schluesener HJ, Unsicker K, Krieglstein K (1997) Bone morphogenetic proteins: neurotrophic roles for midbrain dopaminergic neurons and implications of astroglial cells. Eur J Neurosci 9(8):1699–1709
54. Garthe A, Huang Z, Kaczmarek L, Filipkowski RK, Kempermann G (2014) Not all water mazes are created equal: cyclin D2 knockout mice with constitutively suppressed adult hippocampal neurogenesis do show specific spatial learning deficits. Genes Brain Behav 13(4):357–364. https://doi.org/10.1111/gbb.12130
55. Luo SX, Huang EJ (2016) Dopaminergic neurons and brain reward pathways: from neurogenesis to circuit assembly. Am J Pathol 186(3):478–488. https://doi.org/10.1016/j.ajpath.2015.09.023S0002-9440(15)00646-X
56. Joksimovic M, Awatramani R (2014) Wnt/beta-catenin signaling in midbrain dopaminergic neuron specification and neurogenesis. J Mol Cell Biol 6(1):27–33. https://doi.org/10.1093/jmcb/mjt043mjt043
57. Neubrand VE, Cesca F, Benfenati F, Schiavo G (2012) Kidins220/ARMS as a functional mediator of multiple receptor signalling pathways. J Cell Sci 125(Pt 8):1845–1854. https://doi.org/10.1242/jcs.102764jcs.102764
58. Scholz-Starke J, Cesca F, Schiavo G, Benfenati F, Baldelli P (2012) Kidins220/ARMS is a novel modulator of short-term synaptic plasticity in hippocampal GABAergic neurons. PLoS One 7(4):e35785. https://doi.org/10.1371/journal.pone.0035785
59. Li N, Sarojini H, An J, Wang E (2010) Prosaposin in the secretome of marrow stroma-derived neural progenitor cells protects neural cells from apoptotic death. J Neurochem 112(6):1527–1538. https://doi.org/10.1111/j.1471-4159.2009.06565.xJNC6565
60. Gao HL, Li C, Nabeka H, Shimokawa T, Saito S, Wang ZY, Cao YM, Matsuda S (2013) Attenuation of MPTP/MPP(+) toxicity in vivo and in vitro by an 18-mer peptide derived from prosaposin. Neuroscience 236:373–393. https://doi.org/10.1016/j.neuroscience.2013.01.007S0306-4522(13)00023-7
61. Naz F, Anjum F, Islam A, Ahmad F, Hassan MI (2013) Microtubule affinity-regulating kinase 4: structure, function, and regulation. Cell Biochem Biophys 67(2):485–499. https://doi.org/10.1007/s12013-013-9550-7
62. West T, Stump M, Lodygensky G, Neil JJ, Deshmukh M, Holtzman DM (2009) Lack of X-linked inhibitor of apoptosis protein leads to increased apoptosis and tissue loss following neonatal brain injury. ASN Neuro 1(1):AN20090005. https://doi.org/10.1042/AN20090005e00004